

Constraints on Relic Magnetic Black Holes

Melissa D. Diamond, David E. Kaplan

*Department of Physics & Astronomy,
The Johns Hopkins University, Baltimore, MD 21218, USA
Department of Physics*

E-mail: mdiamon8@jhu.edu, david.kaplan@jhu.edu

ABSTRACT: We present current direct and astrophysical limits on the cosmological abundance of black holes with extremal magnetic charge. Because they don't Hawking radiate, much lighter primordial black holes could exist today if they are extremal. The dominant constraints come from white dwarf destruction for intermediate masses, and intergalactic gas heating for heavier black holes. Extremal magnetic black holes may catalyze proton decay, and thus we derive robust limits – independent of the catalysis cross section – from the above as well as from white dwarf heating. We discuss other bounds such as those from neutron star heating, solar neutrino production, binary formation and annihilation into gamma rays, and magnetic field destruction. We note that stable magnetically charged black holes can assist in the formation of neutron star mass black holes.

¹corresponding author

Contents

1	Introduction	2
2	Extremal Magnetic Black Holes (EMBHs)	3
3	Bounds on EMBHs Without Catalysis	4
3.1	Gas Cloud Heating	4
3.2	White Dwarf Destruction	6
3.3	Binary Mergers and Gamma Ray Emission	12
3.4	Destruction of Large Scale Magnetic Fields	16
3.5	MACRO	17
4	The Effects of Proton Decay Catalysis on EMBH Bounds	17
4.1	Convection in White Dwarfs	19
4.2	White Dwarf Heating	24
4.3	Neutron Star Heating and Background X-Rays	26
4.3.1	Bounds from Overheating Neutron Stars	27
4.3.2	Annihilation Effects and the Superconducting Core	28
4.4	Proton Decay in the Sun, Neutrinos and SuperK	29
4.4.1	Annihilation in the Sun	30
4.5	Direct Constraints	31
5	Non-Extremal Magnetic Black Holes	32
5.1	Gas Heating	32
5.2	White Dwarf Consumption	33
5.3	Neutron Star Collapse	35
6	Conclusion	36
A	EMBH Friction with a Fermi Gas at Finite Temperatures	37
B	Calculation Details for Binary Mergers	38
B.1	Derivation of the Merger Time for a Magnetically Charged Binary	38
B.2	Derivation of the EMBH Binary Merger Rate	41
	Bibliography	44

1 Introduction

A simple and well-motivated extension of the standard model of particle physics (and Maxwell’s equations) is the inclusion of magnetic monopoles. Magnetic monopoles are a natural consequence of grand-unified theories (GUTs) [1, 2], have been searched for by a number of different experiments [3–5], and were even an original motivation for cosmic inflation [6, 7].

One possible manifestation of magnetic charges in our universe could be as magnetically charged black holes. Primordial black holes could have formed in the early universe from, for example, large-amplitude short-wavelength density perturbations or from early phase transitions [8, 9]. If monopoles existed (or perhaps dominated) at that time, one might expect \sqrt{N} fluctuations to leave primordial black holes with magnetic charges. Light enough black holes could eventually Hawking radiate until they become extremal, leaving a magnetically charged remnant until today, a fate different from that of small non-charged black holes. More exotic formation stories may exist, but we will not address those here.

Instead, in this paper, we put constraints on the existence of relic primordial black holes with magnetic charge. We focus on extremal magnetic black holes (EMBHs), but point out the applicability and strength of the bounds in the non-extremal cases (namely, for black holes heavier than 10^{15}g). The dominant bounds come mainly from two sources – galactic gas cloud heating at large masses, and destruction of white dwarfs at moderate and low masses. We also present novel constraints from gamma ray emission for EMBHs at low masses, though there are never dominant. In addition, we discuss bounds from the destruction of magnetic fields, the Parker bound, and direct searches.

Magnetic monopoles derived from some GUTs are predicted to catalyze proton decay with significant cross sections [10, 11]. The bounds on EMBHs change significantly when one assumes catalyzed proton decay in stellar objects – neutron stars, white dwarfs, and the sun – due to heating and neutrino emission. We scan over cross sections for this catalysis to generate robust bounds on relic abundances of EMBHs independent of the size of this effect. The dynamics of nucleon decay near EMBHs are highly non-trivial and we leave a detailed analysis for future work.

This paper is organized as follows. In Section 2, we briefly discuss the relevant physical properties of EMBHs. In Section 3, we describe and summarize bounds due to the annihilation of binary EMBHs, the heating of the intergalactic medium, and the destruction of White Dwarfs, as well as other sources of weaker bounds assuming the catalysis of proton decay is negligible. In Section 4, we include the catalysis of proton decay by EMBHs and scan over all possible physically sensible cross sections. Adding this effect weakens the bounds in some mass regimes by, for example, turning off annihilation in white dwarfs. For illustration, we also show, for a fixed catalysis cross section, bounds as a function of mass and see the effects of new sources of constraints, such as neutron star heating and proton decay in the sun. In section 5 we explore bounds that apply to stable non-extremal magnetic black holes. Finally, we conclude in Section 6. We compare our constraints with those previously determined in [12, 13] in figures 1, and 3 describe them briefly in sections 3.4 and 4.4.

2 Extremal Magnetic Black Holes (EMBHs)

In general relativity, black holes with magnetic charge are described by the Reissner-Nordstrom metric, one that is spherically symmetric and carries an outer event horizon and an inner Cauchy horizon. The extreme limit of the magnetic charge is one in which these horizons merge, producing the metric:

$$ds^2 = -\left(1 - \frac{GM}{r}\right)^2 dt^2 + \left(1 - \frac{GM}{r}\right)^{-2} dr^2 + r^2(d\theta^2 + \sin^2\theta d\phi^2) \quad (2.1)$$

where M is the ADM (asymptotic) mass of the black hole and G is Newton's constant. The EMBH has, in natural units, a magnitude charge

$$Q = \frac{M}{m_P} \quad (2.2)$$

Where $m_P = G^{-1/2} = 1.22 * 10^{19}$ GeV is the Planck mass. In these units, $Q = 10^5$ corresponds to a black hole mass of ~ 1 g. Note that this is a different definition of Q than is given in other works [12, 14] on extremal magnetic black holes. The minimum possible value for Q is set by the Dirac quantization $Q_{min} = \frac{1}{2e}$ [15].

EMBHs have some interesting and unresolved properties. Being extremal, EMBHs will not Hawking radiate, as uncharged black holes are assumed to [16]. Uncharged black holes with masses $M \lesssim 5 * 10^{14}$ g are predicted to decay faster than the age of the universe, while EMBHs are expected to be stable, and thus could in principle be cosmological relics. Recent work [14] suggests that EMBH may also have finite lifetimes if they can decay into magnetic monopoles. The lifetime is model dependent and sensitive to properties of the magnetic monopole, so we will not consider it in this work. In the same work, [14], it was shown that as one approaches an EMBH, there are large regions where the magnetic fields are strong enough to condense electroweak bosons and to restore the Higgs field minimum to its origin, making standard model fermions massless. Interestingly, one would also expect in this region the sphaleron barrier for baryon number violation would disappear [17]. In addition, the interior of non-extremal magnetically charged black holes will have an inner Cauchy horizon with known instabilities [18]. In general relativity, the interior metric can only be extended in physically nonsensical ways (requiring the existence of an infinite number other universes). It is thus expected that new physics lives at this horizon, and in the extremal limit, it is reasonable to expect that the new physics lives at $r = GM$. The physics at this surface, for example, could be of Planckian density [19] and may or may not violate baryon number in a significant way, and may in general source other fields (black hole 'hair'). Thus significant model dependence dictates the physics at close ranges.

A possibly important feature of EMBHs is their potential for catalyzing proton decay, akin to that in GUT-induced magnetic monopoles, [10, 11]. It is a non-trivial question here – not only is there model dependence with respect to the properties of the core of the EMBH, but the path to the core for a charged particle will involve gauge-boson interactions at medium and long distances and gravitational and (potentially) black-hole hair interactions

at short distances¹. A full analysis for specific models of EMBHs would be interesting. However, to put a robust bound on these objects, we will allow the proton catalysis cross section to be a free parameter (within reason), and will see it is possible to put more *model-independent* limits from various astrophysical phenomena.

We also note that a number of other interesting properties of EMBHs were explored in [14]. For one, charged fermions near an EMBH will experience radically different dynamics. In regions where the magnetic field is larger than the fermion’s squared mass, the low-lying energy quantum states are Landau levels and should be those of two-dimensional fermion states which move radially and have degeneracy of order Q . This degeneracy is predicted to lead to an enhanced Hawking decay rate of non-extremal black holes by a factor of Q . This will have some effect on the discussion of bounds on merger rates.

3 Bounds on EMBHs Without Catalysis

Relic EMBHs are heavy magnetic charges which are expected to be non-relativistic at all relevant times and to follow the dark matter distribution, at least once they are decoupled from the plasma. Physical effects from these objects include gas heating, white dwarf destruction, magnetic field destruction, and high-energy particle emission from annihilation. We describe the bounds from these effects in the subsections below and summarize the results of these effects as constraints on the relic abundances of EMBHs via the parameter f , the average relic density of EMBHs over the average dark matter energy density, $f \equiv \rho_{bh}/\rho_{dm}$, with $\rho_{dm} = 0.3 \text{ GeV cm}^{-3}$. In this section, we are ignoring the possibility of proton-decay catalysis, leaving it for the next section. We plot the bounds (without catalysis) for a range of masses in Figure 1.

3.1 Gas Cloud Heating

When an EMBH passes through an ionized plasma, it loses energy by exciting long range eddy currents. The energy lost by the EMBH is deposited into the plasma via kinetic energy of the accelerated electrons. This heats the plasma. Observations of the temperature and cooling rate of warm ionized gas clouds in the Milky Way place constraints on the EMBH abundance. We limit the EMBH abundance to be low enough that they do not change the observed temperature of clouds of warm ionized medium in the Milky Way. We do this by requiring that the heating rate from friction be less than the average cooling rate determined in a survey of the warm ionized medium [20].

The friction between a magnetic monopole and a plasma is described in [21]. We adapt it here for an EMBH with charge Q

$$\left(\frac{dE}{dx}\right)_p = -\frac{16\pi^{1/2}e^2n_e}{3\sqrt{2Tm_e}}Q^2v\left[\ln(4\pi n_e L_D^2 l) + \frac{2}{3}\right] \quad (3.1)$$

¹For example, an extremal magnetic black hole should gravitationally repel an electrically charged particle with a large charge to mass ratio (*e.g.*, the proton), as the end result would be super-extremal. This would also be true of particles with spin.

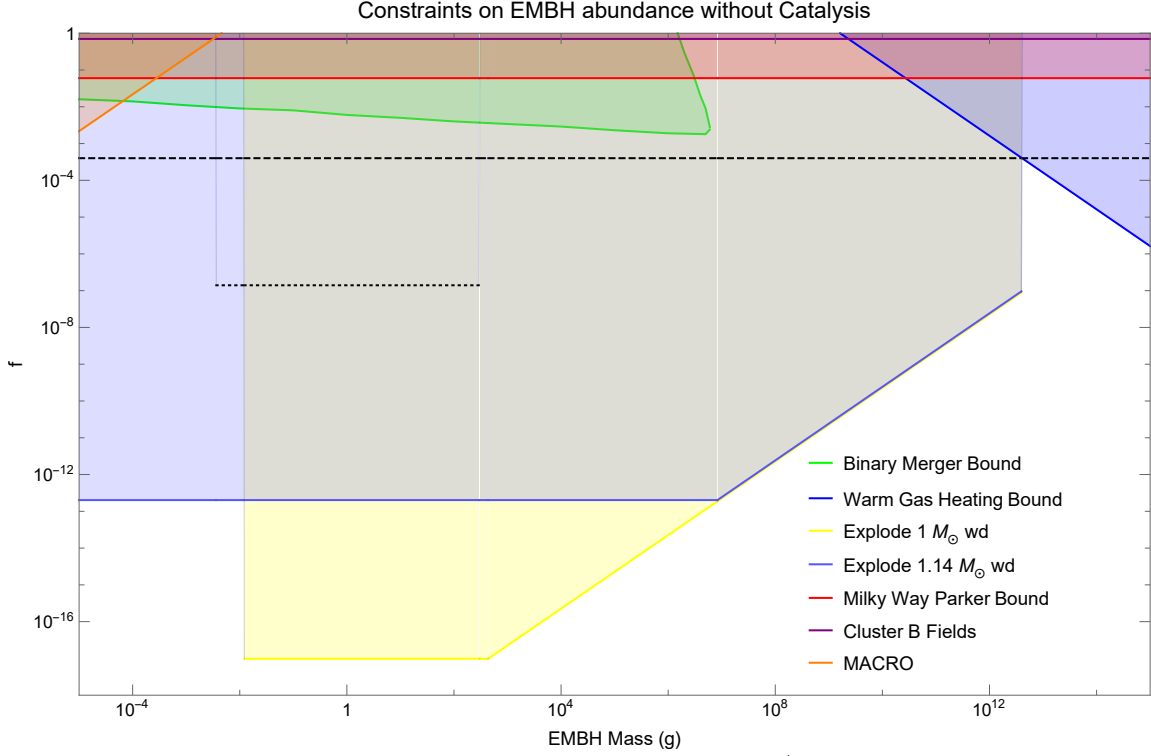


Figure 1: These are the bounds on the EMBH abundance $f \equiv \rho_{bh}/\rho_{dm}$ if nucleon catalysis effects, which are described in section 4, are not considered. Shaded regions are ruled out. The green region is ruled out by γ -rays emitted from binary mergers, described in more detail in Section 3.3. The yellow and light blue regions are ruled out by the existence of 1 Gyr old non magnetic $1 M_{\odot}$ white dwarfs and by WD J0551+4135 a $1.14 M_{\odot}$ CO white dwarf respectively. EMBHs can destroy these white dwarfs by annihilating inside of them. This is described in more detail in 3.2. The dark blue region is ruled out by EMBH overheating warm ionized gas clouds in the Milky Way. This effect is further explained in Section 3.1. The red and purple regions are ruled out by EMBH interaction with large scale magnetic fields, which is described in 3.4. The orange region is ruled out by observations made by the MACRO detector and described in 3.5. For comparison we show the previously established EMBH bounds set by Bai et al in [12] in black. The dashed bound comes from the Parker effect in the Andromeda Galaxy, and the dotted one comes from EMBHs annihilating in the sun and producing a neutrino signal visible at Super K. We do not show the full extent of the latter bound because of uncertainty around how convection in the sun will impact the annihilation rate for EMBHs with $M > 300$ g.

Where n_e is the electron number density, T is the gas temperature, v is the velocity of the monopole, $L_D = \sqrt{\frac{T}{4\pi n_e e^2}}$ is the plasma Debye length, and $l = \left(\frac{2T}{\pi m_e}\right)^{1/4} \frac{1}{v^{1/2} \omega_p}$ is the attenuation length of the plasma with plasma frequency $\omega_p = \sqrt{\frac{4\pi e^2 n_e}{m_e}}$.

Ionized gas clouds observed in this cooling survey [20] have an average $n_e \sim 0.08 \text{ cm}^{-3}$ and temperatures of about $T \sim 6000 \text{ K}$. Using (3.1) we find that a single EMBH moving through at virial velocity $v \sim 10^{-3}$ will deposit energy into the plasma at a rate

$$\frac{dE}{dt} = 9 \times 10^{-3} \left(\frac{M}{10^9 \text{ g}} \right)^2 \text{ erg s}^{-1} \quad (3.2)$$

Unregulated by cooling, this could significantly change the temperature and behavior of the gas in a time $\delta t \sim \frac{T}{dT/dt} \sim 1 \text{ Myr} \left(\frac{10^9 \text{ g}}{M} \right) \frac{1}{f}$. This indicates that a wide range of EMBH can change the properties of the warm ionized medium in the Milky Way in a time comparable to that of other less exotic heating processes already present in the Milky Way [22].

The temperature of warm ionized gas clouds in the Milky Way is regulated by a variety of heating and cooling processes. The primary cooling process is electron and hydrogen atom collisions with singly ionized carbon atoms. These collisions can excite fine structure transitions in the ground state of carbon atoms from the $^2P_{1/2}$ state to the $^2P_{3/2}$ state. Observations of infrared emission from de-excitations of these excited carbon atoms are used to estimate the cooling rates in ionized gas clouds [20]. The cooling rate is sensitive to the temperature of the gas cloud. The heating rate of the gas cannot be directly inferred but is estimated based on the cooling rate [20]. Given that EMBH heating can change the temperature of the gas rather quickly, the heating rate by passing EMBHs should not exceed the observed cooling rate. Doing so would disturb the observed dynamics of the gas, and change both its temperature and its cooling rate.

Cooling rates for a variety of warm ionized gas clouds are reported in [20]. The cooling rates are grouped by the velocity of the gas cloud. We compare the EMBH gas heating rate to the cooling rate for low velocity gas clouds, because this group puts the strongest bounds on EMBHs.² The average cooling rate is $(dE/dt) \sim n_H \times 10^{-25.65 \pm 0.11} \text{ erg s}^{-1}$ where $n_H \sim 0.25 \text{ cm}^{-3}$ is the number density of hydrogen atoms in a typical warm ionized cloud [20, 22]. The rate is shown with 3σ uncertainties. Requiring that EMBH heating not exceed the 3σ upper limit in the cooling rate gives the following constraint on the relic abundance of EMBHs:

$$f \lesssim 1.6 \times \left(\frac{M}{10^9 \text{ g}} \right)^{-1} \left(\frac{n_H}{0.25 \text{ cm}^{-3}} \right). \quad (3.3)$$

This bound is only sensible if there is a large enough abundance of EMBHs in a warm gas cloud to consistently heat it. For EMBHs that make up f of the dark matter, there are $\sim 10^{31} \frac{f}{M/\text{g}} \text{ pc}^{-3}$ in the galaxy. Warm ionized gas clouds have a typical radius of $\sim 2 \text{ pc}$, indicating that all such gas clouds would be well populated by EMBHs with masses at least up to 10^{15} g [22]. Gas heating effects for EMBHs with masses above 10^{15} g is discussed in section 5.1

3.2 White Dwarf Destruction

The hot, dense conditions inside of Carbon-Oxygen (CO) white dwarfs make them very sensitive to small energy injections [23]. For example, depositing $\sim 6 \times 10^{21} \text{ GeV}$ within a region of radius of $\sim 6 \times 10^{-3} \text{ cm}$ in a time less than $\sim 3 \times 10^{-12} \text{ s}$ leads to runaway fusion in white dwarfs with masses above $1M_\odot$, destroying the white dwarf in a supernova explosion [23–25]. We will use this sensitivity to put bounds on EMBH densities from the observation of old white dwarfs in the galaxy.

²In principle, a somewhat stronger bound can be found using high velocity gas clouds, however there is significant uncertainty around n_e in these gas clouds making it difficult to compare the cooling rate to the heating rate from EMBH.

EMBHs collect inside of white dwarfs, and can eventually merge and annihilate. The EMBHs release a large amount of electromagnetic energy when they merge, typically more than enough to destroy the white dwarf. The bounds come from limiting the EMBH abundance to be low enough that the white dwarfs we consider do not get destroyed within the first Gyr of their life.

The amount of energy deposited needed to destroy a white dwarf depends on the white dwarf’s mass, with lower mass white dwarfs requiring larger energy deposits to initiate runaway fusion. Not all EMBHs have enough mass energy to destroy all white dwarfs. To account for this we consider bounds from two different sets of white dwarfs: a collection of known $1M_{\odot}$ white dwarfs, and WD J0551+4135, a $1.14M_{\odot}$ white dwarf thought to have formed from the collision of two smaller CO white dwarfs[26].

We set limits using $1M_{\odot}$ white dwarfs because hundreds of CO white dwarfs with masses around $1M_{\odot}$ have been observed [27]. Their average cooling age is 1.9 Gyr, though the oldest such white dwarfs have cooling ages over ~ 10 Gyr [27]. EMBHs destroying $1M_{\odot}$ within the first Gyr of their existence would eliminate more than half of these white dwarfs even allowing for some uncertainty in their exact cooling ages. White dwarfs that form with starting masses above $1.05M_{\odot}$ are thought to be Oxygen-Neon (ONe) white dwarfs [28], which require much larger energy depositions to trigger runaway fusion [23] and ultimately do not give useful bounds. $1M_{\odot}$ white dwarfs are among the highest mass white dwarfs (having the smallest trigger energy) that can be safely assumed to be made of carbon and oxygen.

We also consider bounds from WD J0551+4135 because it is a rare CO white dwarf with a mass above $1.05M_{\odot}$. WD J0551+4135 is a $1.14M_{\odot}$ white dwarf thought to have formed from the collision of two smaller CO white dwarfs a bit over 1 Gyr ago [26]. It’s high mass makes it’s trigger energy low enough that EMBH’s too light to trigger runaway fusion in $1M_{\odot}$ white dwarfs can destroy it. Key physical properties of these white dwarfs used for calculations are shown in Table 1.

While the physical details of these white dwarfs may differ, the process of capturing EMBHs that sink to the core, merge, and initiate runaway fusion is shared between them.

White dwarfs are composed of a degenerate Fermi gas of electrons. A magnetic monopole passing through a degenerate Fermi gas will deposit energy into it by inducing eddy currents. Within a certain mass range, an EMBH passing through a white dwarf can lose enough energy to get trapped inside the stellar remnant.

An EMBH passing through a white dwarf will interact both with the carbon ion plasma in the star and the electron Fermi gas. The stopping power of a degenerate Fermi gas at zero temperature for a monopole is given in [29]. Adapting their result to accommodate an EMBH, we find:

$$\frac{dE}{dx} = \frac{GM^2\omega_p^2v}{v_f} \left[\ln \frac{4E_f}{\nu_{\sigma}^{ei}} - \frac{1}{2} \right] \quad (3.4)$$

where again, ω_p is the plasma frequency, v is the velocity of the passing monopole, v_f is the fermi velocity, E_f is the Fermi energy, and $\nu_{\sigma}^{ei} \sim 10^{17} \text{ s}^{-1}$ is the electron ion scattering frequency [30] at relevant white dwarf densities and temperatures [31] (we use 10^6 g/cm^3

$M_{wd} (M_{\odot})$	1	1.14
$R_{wd} \text{ (km)}$	5600	4600
$\rho_c \text{ (g/cm}^3\text{)}$	2.9×10^7	7×10^7
$E_T \text{ (GeV)}$	7×10^{21}	3×10^{19}
$\tau_{diff} \text{ (s)}$	3×10^{-12}	6×10^{-13}
$B_c \text{ (kG)}$	1	50
$M_{min} \text{ (g)}$	0.012	2×10^{-5}
$M_{Th} \text{ (g)}$	2600	5×10^7
$M_{max} \text{ (g)}$	4×10^{12}	4×10^{12}

Table 1:

Observed and derived properties of the white dwarfs used to derive bounds in this paper, where R_{wd} is the radius in km, ρ_c is the density of the white dwarf core in g/cm³, E_T is the threshold energy needed to initiate runaway fusion in the white dwarf in GeV, τ_{diff} is the diffusion time in seconds, and B_c is the maximum the magnetic field at the white dwarf core. The EMBH masses M_{min} , M_{Th} , and M_{max} are (in grams) the minimum mass needed to trigger runaway fusion, the threshold mass required to overcome the white dwarf core magnetic field, and the maximum mass that can sink to the core in less than a Gyr, respectively. The first column is for generic non-magnetic 1 M_{\odot} CO white dwarfs and the second is for WD J0551+4135, a 1.14 M_{\odot} CO white dwarf that resulted from the collision of two smaller CO white dwarfs. The radius and density are derived using white dwarf density profile information found in Appendix D of [25], and the diffusion time is from the same reference. The B_c value is our estimate for the magnetic field at the white dwarf core based on observations (or lack thereof) of the magnetic field on the white dwarf surface.

and $10^{6.8}$ K respectively). For these parameters the slowing rate is about

$$\frac{dE}{dx} \simeq 1.1 \times 10^{18} \times \left(\frac{\rho_{wd}}{10^6 \text{ g cm}^{-3}} \right) \left(\frac{M}{g} \right)^2 \left(\frac{v}{2.3 \times 10^{-2}} \right) \text{ GeV/km.} \quad (3.5)$$

where the velocity is scaled with the escape velocity at the surface. We use the escape velocity at the surface of a $1M_{\odot}$, $v_{esc} \sim 2.3 \times 10^{-2}$ for illustrative purposes.

The above description of the friction is appropriate when the energy gained by electrons passing the monopole, $\sim pv(\cos(\theta) - \cos(\theta'))$, is large compared to the temperature of the fermi gas. Here, p is the momentum of passing electrons, θ is the angle between the velocity of the incoming electron and v , and θ' is the angle between the scattered electron and v . When the energy gained by passing electrons is small compared to the temperature of the fermi gas, finite temperature effects must be considered. The stopping power for a magnetic monopole in a fermi gas with a non zero temperature is derived in Appendix A, and shown here.

$$\left(\frac{dE}{dx} \right)_f = \frac{Ge^2 \sqrt{2m_e} M^2}{\pi^2} \text{Log} \left[\frac{2E_f}{\nu_{\sigma}^{ei}} \right] \times \int_{-1}^1 \int_{-1}^1 \int_0^{\infty} \sqrt{E} \times f(E) (1 - f(E + \Delta E)) dx dy dE \quad (3.6)$$

where

$$f(E) = \frac{1}{\exp \left(\frac{E - E_f}{T} \right) + 1} \quad (3.7)$$

and

$$\Delta E = pv(x - y) \quad (3.8)$$

. The total friction on EMBHs traversing a white dwarf can be estimated by combining the contributions from (3.6) and (3.1) for a plasma of carbon nuclei. We performed this calculation numerically.

The lightest EMBHs we consider, $M \sim 2 \times 10^{-4} \text{ g} \sim 10^{20} \text{ GeV}$, have kinetic energies within the galaxy of $\sim 6 \times 10^{13} \text{ GeV}$. Using (3.5) to make a simplified estimate of the energy lost by an EMBH traversing a white dwarf one finds that even the lightest EMBHs under consideration lose enough energy to get trapped inside the white dwarf after traversing about $\sim 1000 \text{ km}$ inside the white dwarf. Heavier EMBHs will lose their kinetic energy in shorter distances, and thus all EMBHs that traverse the white dwarfs considered here will become gravitationally bound to them.

The rate at which a white dwarf accumulates EMBHs, Γ_{wd} , can be found simply with a Sommerfeld enhanced cross section:

$$\Gamma_{wd} \simeq \left(\frac{\rho_{dm} f}{M} \right) \pi R_{wd}^2 \frac{v_{esc}^2}{v} \sim 2.7 * 10^{20} f \left(\frac{M}{g} \right)^{-1} \left(\frac{R_{wd}}{5600 \text{ km}} \right)^2 \left(\frac{v_{esc}}{2.3 * 10^{-2}} \right)^2 \text{ Gyr}^{-1} \quad (3.9)$$

where R_{wd} and v_{esc} are the white dwarf's radius and escape velocity, respectively.

Once inside a white dwarf, EMBHs must sink to the core in order to find each other and annihilate. The core density of the white dwarf, the core magnetic field, and the EMBH mass all dictate how an EMBH will behave once inside of the white dwarf. For example, the core magnetic field separates lighter EMBHs of opposite charge preventing them from annihilating initially, while heavier EMBHs can overcome the magnetic field and their behavior will be determined by friction within the white dwarf.

In order to annihilate, light EMBHs first sink to a place where the magnetic gravitational and mutually attractive forces between opposite charge EMBHs balance. The strength, prevalence, and structure of white dwarf magnetic fields remains an area of active research. The surface magnetic field of WD J0551+4135 has been measured to be $\sim 50 \text{ kG}$ [26]. Current measurement techniques are only sensitive to surface magnetic fields of $\sim 1 \text{ kG}$ or higher [32]. When considering $1 M_{\odot}$ white dwarfs, we will only use those whose magnetic fields were too small to measure with current technology $\lesssim 1 \text{ kG}$. White dwarf magnetic fields are only measured at the surface. We will estimate that the core magnetic field is equal to the observed surface field. Magnetic fields in white dwarfs are thought to be fossil fields left over from the star they came from, or the result of differential rotation between proto-white dwarfs in a binary system and the common envelope they formed in [33]. In the former case, the white dwarf magnetic field arises from conserving the magnetic flux of the larger star it came from. Modeling indicates that the poloidal fossil field must be supported by a twisted toroidal field outside of the core to survive over long times scales [34]. In the latter case the magnetic field comes from a magnetized accretion disk, which accretes onto the surface of the white dwarf [35]. In both cases the magnetic field is generated well outside of the core. Thus, there is no reason to expect the core field to be much larger than the surface field, justifying our assumption.

If a sufficiently strong poloidal magnetic field is present in the core, EMBHs will separate into two oppositely charged surfaces on opposite sides of the white dwarf center. EMBHs of the same charge do not interact strongly and we ignore their interaction. One can estimate where these EMBHs will settle by finding the zeros in the derivative of the expression for the potential energy of EMBHs near a white dwarf core.

$$-B_{int} \frac{M}{m_P} + \frac{4\pi r}{3} \frac{\rho_c}{m_P^2} M + 2 \frac{M^2(N-1)}{m_P^2(2r)^2} = 0 \quad (3.10)$$

Here B_{int} is the magnetic field at the center, ρ_c is the local density, m_P is the planck mass, and N is total number of EMBHs in the core, which we assume are split evenly by charge. Note that the attraction that one EMBH feels toward the cluster of oppositely charged EMBH is enhanced by 2 due to the combined magnetic and gravitational attraction. If only one EMBH is present in the star it will settle at $r = \frac{3}{4\pi} \frac{B_{int} m_P}{\rho_{wd}}$, which for a $1 M_\odot$ white dwarf with a core density of $\sim 3 \times 10^7$ g/cm³ and a core magnetic field strength of 1 kG is $r \sim 0.03$ cm. We numerically solve for the time needed to reach this region using (3.4) and a density profile derived from the equations presented in Appendix D of [25] and find all EMBHs light enough to be separated by the core magnetic field sink to their equilibrium point in less than about 6×10^{11} s, well under 1 Gyr.

As N increases, the stable solution to (3.10) will move closer to the center. Eventually, Equation (3.10) has no real solution, indicating that EMBHs simply fall to the center of the white dwarf instead of separating into polarized regions. This happens when

$$B_{int} < \min \left[\frac{4\pi r}{3} \frac{\rho_{wd}}{m_P} + \frac{1}{4} \frac{M(N-1)}{m_P r^2} \right] \quad (3.11)$$

where 'min' means the minimum value as a function of r . Therefore EMBHs of opposite sign will fall toward the center of the white dwarf, and thus each other, when

$$\frac{B_{int}^3 m_P^3}{3\pi^2 \rho_{wd}^2} < M(N-1) \quad (3.12)$$

or

$$2.2 \times 10^2 g \left(\frac{B_{int}}{10^3 G} \right)^3 \left(\frac{10^8 \text{gcm}^{-3}}{\rho_{wd}} \right)^2 < M(N-1) \quad (3.13)$$

thus setting a threshold for the total accumulated EMBH mass which must be reached for annihilations to be possible. One can check that EMBHs in separated clusters moving at thermal velocity in the white dwarf core do not have enough kinetic energy to traverse the energy barrier between opposite charged clusters until (3.13) is satisfied. When (3.13) is satisfied, mutual attraction between the EMBH clusters will dominate over other forces acting on them. Annihilation proceeds quickly once the magnetic field barrier is overcome. Only a single annihilation is needed to destroy the white dwarf.

EMBHs heavier than the threshold mass set in (3.13) will be strongly enough attracted to opposite charges to overcome the force of the core magnetic field. These EMBHs will be able to fall toward each other and interact when their mutual attraction becomes stronger than their gravitational attraction to the white dwarf core. This happens once they fall

within a radius $r_* \simeq \left(\frac{3M}{8\pi\rho_{wd}}\right)^{1/3} \sim 9 \text{ cm} \left(\frac{M}{10^{12}\text{g}}\right)^{1/3} \left(\frac{10^8\text{gcm}^{-3}}{\rho_{wd}}\right)^{1/3}$. We numerically found that, for both the $1 M_\odot$ white dwarfs and for the $1.14 M_\odot$ white dwarf, the time EMBH need to sink to r_* scales approximately linearly with the mass, with $4 \times 10^{12} \text{ g}$ being the heaviest EMBHs that can reach the core within a Gyr. EMBHs with masses above this do not sink quickly enough to annihilate, and those with masses below $4 \times 10^{12} \text{ g}$ will sink quickly compared to a Gyr.

The angular momentum and energy of the EMBH will not be conserved in the high friction environment inside of the white dwarf, and thus EMBHs sink directly to r_* and then only need to traverse r_* to meet and annihilate. EMBHs will begin to accelerate toward each other once they enter r_* . We can conservatively estimate the time they need to reach each other as r_*/v_* , where v_* is the velocity at which EMBHs move once they have entered r_* . v_* is calculated numerically, but scales roughly linearly as $v_* \sim 10^{-21}(M/10^{12}\text{g})^{-1}$ in the $1.14 M_\odot$ white dwarf. v_* will be faster inside of the $1 M_\odot$ white dwarfs due to their lower core density. Even the heaviest slowest moving EMBHs that make it to the core in under a Gyr, can pair and annihilate in well under a Gyr.

When two opposite charge EMBHs collide, they release energy through a magnetic "chirp" during the collision and potentially through Hawking radiation of the non extremal black hole left behind after the collision. The magnetic dipole they represent vanishes in about $t_s \sim 2r_s = 4GM \sim 10^{-38}\left(\frac{M}{\text{g}}\right) \text{ s}$, the time it would take an electromagnetic signal to traverse the Schwarzschild radii of the two EMBHs when they first make contact. One can expect an electromagnetic "chirp" from the sudden changing and rearranging of the magnetic field akin to the gravitational chirp that happens during the final moments of an uncharged binary merger and the subsequent ringdown. A magnetic dipole p will radiate energy at a rate $P = \frac{2}{3}\left(\frac{d^2p}{dt^2}\right)^2$. Just before colliding, two EMBHs separated by a distance $2r_s$ will form a dipole with a dipole moment $2r_s * Q \sim 4\frac{M^2}{m_p^3}$. If this dipole were to suddenly disappear in t_s then a burst of $\frac{2}{3}M \sim 3.7 \times 10^{23}\left(\frac{M}{\text{g}}\right) \text{ GeV}$ of electromagnetic energy will be emitted over t_s . The energy needed to destroy each of the white dwarfs is shown in Table 1. From the "chirp" alone any EMBH with a mass above $\sim 0.02 \text{ g}$ easily furnish the energy needed to destroy a $1M_\odot$ white dwarf, and any EMBH heavier than $\sim 8 \times 10^{-5} \text{ g}$ can supply the energy needed to destroy WD J0551+4135.

Lighter EMBHs can also supply enough energy to destroy a white dwarf through the Hawking radiation from the non-extremal remnant left behind after the merger. [25] suggest a black hole of mass M inside of a white dwarf will Hawking radiate at a rate of $\sim 1.4 \times 10^{37} \text{ GeV fs}^{-1}\left(\frac{M}{\text{g}}\right)^{-2}$. We assume the EMBHs involved in the merger had masses which were $\mathcal{O}(1)$ the same. The remnant left behind would then be about $\mathcal{O}(1)$ non extremal, and need to lose $\sim M$ in mass to get back down to an extremal mass. Such black holes radiate at nearly the same rate as uncharged black holes do, and may radiate even faster if we consider Q enhancements to the decay rate described in [12, 14]. Assuming the merger remnant radiates of a mass M at a rate of at least $\sim 1.4 \times 10^{37} \text{ GeV fs}^{-1}\left(\frac{M}{\text{g}}\right)^{-2}$, then EMBHs with masses as low as 0.012 g for $1 M_\odot$ white dwarfs and $2 \times 10^{-5} \text{ g}$ for WD J0551+4135 will be able to supply the energy needed to destroy their host white dwarf.

We set a bound on light EMBHs by requiring that their abundances are low enough to prevent white dwarfs from accumulating the threshold mass of EMBHs needed to overcome the magnetic field barrier within 1 Gyr. For EMBHs with masses above this threshold, the bound is set by requiring the white dwarf not accumulate 6 EMBHs in 1 Gyr. Once there are 6 charges present, there is a $> 95\%$ chance that one of the EMBHs is of the opposite charge as the others, and able to annihilate. The existence of hundreds of non-magnetic, white dwarfs with masses around $1 M_\odot$, and cooling ages longer than 1 Gyr, and no apparent suppression in the number of these white dwarfs based on age or mass [27], rules out all of EMBH parameter space where annihilation within 1 Gyr would be expected. For the $1 M_\odot$ white dwarfs this bound is

$$f < \begin{cases} 1 \times 10^{-17} & 0.012 \text{ g} \leq M \leq \frac{1}{6} \times 2.6 \times 10^3 \text{ g} \\ 2.3 \times 10^{-20} \left(\frac{M}{\text{g}}\right) & \frac{1}{6} \times 2.6 \times 10^3 \text{ g} < M < 4 \times 10^{12} \text{ g} \end{cases} \quad (3.14)$$

and for WD J0551+4135 this is

$$f < \begin{cases} 2 \times 10^{-13} & M \leq 5 \times 10^7 / 6 \text{ g} \\ 2.4 \times 10^{-20} \left(\frac{M}{\text{g}}\right) & 5 \times 10^7 / 6 \text{ g} < M < 4 \times 10^{12} \text{ g} \end{cases} \quad (3.15)$$

3.3 Binary Mergers and Gamma Ray Emission

Oppositely charged EMBHs can form binary systems in the early universe when they would have been packed together much more tightly than today. These binaries eventually spin down and merge. Assuming the EMBHs involved in the merger have $\mathcal{O}(1)$ the same charge, the merger will leave behind a new non-extremal black hole. The new black hole will have lost a 'chirp mass' fraction of its mass to electromagnetic and gravitational radiation and then, unprotected by an extremal charge, could rapidly Hawking radiate until it decays down to its new extremal mass. Conservatively, we assume it will radiate off about $\sim M$, the mass of the EMBHs contributing to the merger. The hot radiation from these merger remnants gets reprocessed by the thermal bath, and ultimately reaches Earth as a γ -ray signal. We can place constraints on EMBH abundance by limiting the γ -ray signal from their merger remnants to be less than 2σ above the diffuse extra-galactic γ -ray flux reported in the most recent isotropic background analysis of data collected by the Fermi-LAT Telescope [36].

Each binary decouples from the Hubble flow when the free fall velocity of the EMBH toward each other exceeds the Hubble velocity pulling them apart. The unique redshift, z_d , when a binary decouples from the Hubble flow and begins spiraling inward is determined by the co-moving separation between the EMBHs, x , and by the mass of the EMBHs involved in the binary. The time it takes for a binary to merge, t_m , is determined by x , z_d , and by the distance y to the next nearest EMBH to the binary. EMBHs do not interact strongly with other EMBHs of the same sign charge, so the next nearest one will only interact with one EMBHs in the binary. The next nearest EMBH will tug one of the in-falling EMBHs out of its free fall path causing the newly decoupled system to form an eccentric binary instead of immediately annihilating in a head on collision. The closer the next nearest EMBH is, the

smaller the eccentricity of the binary system will be. Less eccentric binaries take longer to spin down. This is how y influences t_m . Together all of this sets the merger rate per black hole for a given redshift $\Gamma_m(z)$ which is derived in full in Appendix B.2.

Once a binary merges, it will produce a sub-extremal black hole that will begin decaying. An uncharged black hole will decay away in a time [16, 25]

$$t_{bh} \sim \frac{15360\pi}{153/8} \frac{M^3}{m_P^4} \sim 1.3 \times 10^{-26} \left(\frac{M}{g}\right)^3 s \quad (3.16)$$

which is a reasonable estimate for the time an $\mathcal{O}(1)$ non-extremal magnetically charged black hole needs to decay down to it's near-extremal mass (this is, in fact, an over estimate, as we only included degrees of freedom up to MeV). This is fast compared to the age of the universe for all black holes constrained by radiation from this decay (roughly $\lesssim 10^7$ g), so it is reasonable to treat the entire decay as happening at the instant the merger happens. Recent works [12, 14] suggest that the decay rate for non-extremal magnetic black holes is enhanced by a factor of the black hole charge, Q , This would reduce the decay time by $\frac{1}{Q}$, which would make it even more reasonable to treat all decays as happening instantaneously.

Sub-extremal black holes in this mass range radiate both electromagnetically and hadronically. The hadronic radiation quickly fragments into more stable particles including neutral pions. The neutral pions then decay into 2 photons. A γ -ray signal also comes from both the photons radiated directly from the black hole, and from those resulting from pion decays. We estimate the combined photon spectrum $\frac{d^2 N_\gamma}{dE_\gamma dt}$ using the derived analytic expressions for a decaying black hole's photon spectra found in equations (30)-(37) of [37]. While the merger remnant is still $\mathcal{O}(1)$ non-extremal it will radiate with approximately the same surface temperature as a non-magnetic black hole. We estimate the total photon spectrum produced during this decay as $\frac{dN_\gamma}{dE_\gamma} \simeq t_{bh} \frac{d^2 N_\gamma}{dE_\gamma dt}$ as the black hole will radiate most of it's energy in this time and around its initial mass.

Photon-photon interactions with CMB photons and Inverse Compton scattering off of electrons reprocess the resulting photon energy distribution from that injected from the initial binary annihilation. The reprocessed γ -ray spectral energy distribution (number of photons per unit energy injected per unit energy interval) $L(E_\gamma, z)$ for injected energies above the reprocessing threshold energy $E_{th} = \frac{36000}{1+z}$ GeV, has the form [38, 39]

$$L(E_\gamma, z) = \begin{cases} 0.767 E_{th}(z)^{-0.5} E_\gamma^{-1.5} & E_\gamma \leq 0.04 E_{th}(z) \\ 0.292 E_{th}(z)^{-0.2} E_\gamma^{-1.8} & 0.04 E_{th}(z) < E_\gamma < E_{th}(z) \end{cases} \quad (3.17)$$

Where E_γ is the energy of the photon. Photons with energy below E_{th} free stream to Earth [39], while those at higher energies are reprocessed. A total reprocessed energy spectrum can be found by multiplying $L(E_\gamma, z)$ by the amount of energy radiated above E_{th} . The shape of the spectrum is independent of the amount of energy injected above E_{th} . The parts of the initial spectra, $(dN_\gamma/dE_\gamma)_{init}$, that were and were not reprocessed combine to give a total visible spectrum of

$$\left(\frac{dN_\gamma}{dE_\gamma}\right)_{tot}(E_\gamma, z) = \begin{cases} \left(\frac{dN_\gamma}{dE_\gamma}\right)_{init} + L(E_\gamma, z) \int_{E_{th}}^\infty \left(\frac{dN_\gamma}{dE'_\gamma}\right)_{init} E'_\gamma dE'_\gamma & E_\gamma \leq E_{th}(z) \\ 0 & E_\gamma > E_{th}(z) \end{cases} \quad (3.18)$$

The flux per unit energy of γ -rays that reach earth can be found by convoluting the reprocessed γ -ray spectrum with the merger rate as a function of redshift:

$$F_\gamma(E_{\gamma 0}) = \frac{\rho_{dm} f}{4\pi} \int_0^{z_m} \frac{1}{H(z)} \Gamma_m(z) \left(\frac{dN_\gamma}{dE_\gamma}\right)_{tot}(E_{\gamma 0}(1+z), z) dz \quad (3.19)$$

where $H(z)$ is the Hubble rate at z , and $E_{\gamma 0}$ is the photon energy today, $\Gamma_m(z)$ is the merger rate per black hole at z . $z_m = \sqrt{\frac{E_{th}(z=0)}{E_{\gamma 0}}} - 1$ is the highest redshift at which a photon could be emitted and still reach Earth with $E_{\gamma 0}$. Any photon with $E_{\gamma 0}$ that reaches Earth today must have been emitted at a redshift $z < z_m$ because energetic photons emitted at earlier times will be reprocessed and redshifted down to lower energies. The total flux per Fermi energy bin is found by integrating $F_\gamma(E_{\gamma 0})$ over the energy range for each bin. We require the integrated γ -ray fluxes to be less than the 2σ upper bound observed by Fermi. The strongest constraints come from the highest energy bin, 580 GeV-820 GeV.

We have, so far, neglected friction of EMBHs with the thermal bath. As explained in Section 3.1, EMBHs interact strongly with plasmas such as the thermal bath. The friction slows infalling EMBHs in binaries, causing them to decouple at later times, and get stretched further apart by the Hubble flow. The extra stretching from staying in the Hubble flow longer reduces the number of binaries that form, and causes those that do to merge at later times. The result is that binaries made of EMBHs that are still strongly interacting with the thermal bath at z_d , their friction-free decoupling redshift, do not significantly contribute to the merger γ -ray signal, and do not significantly contribute to the EMBH abundance bound. We consider an EMBH to be strongly interacting with the thermal bath when friction with the thermal bath more strongly influences their velocity than Hubble acceleration does, $(\frac{dE}{dx})_f / (MV) > H(z)$.

Because the frictional force grows as M^2 , heavier EMBHs are more strongly affected by friction with the thermal bath than lighter ones are. Friction begins to weaken the bound for EMBH with masses above $10^6 g$, and removes it entirely for EMBH with masses above $10^7 g$.

The bounds are shown in Figure 2. The most notable feature in Figure 2 is that the bounds bend backward, weakening at higher f for EMBH with masses $10^6 - 10^7 g$. This happens because increasing f decreases the typical spacing between EMBH. This reduces the distance between a binary and the next nearest EMBH, which lowers the typical binary eccentricity. This effect is normally insignificant, but becomes important when friction reduces the number of binaries contributing to the bound. Friction is strongest at earlier times when the thermal bath was more dense. Less eccentric binaries need more time to merge, and must decouple at earlier times to merge at $0 \geq z > z_m$. These less eccentric binaries are the ones most affected by friction. As the EMBH mass increases, an increasing fraction of binaries that would decouple without friction instead get pulled apart by it.

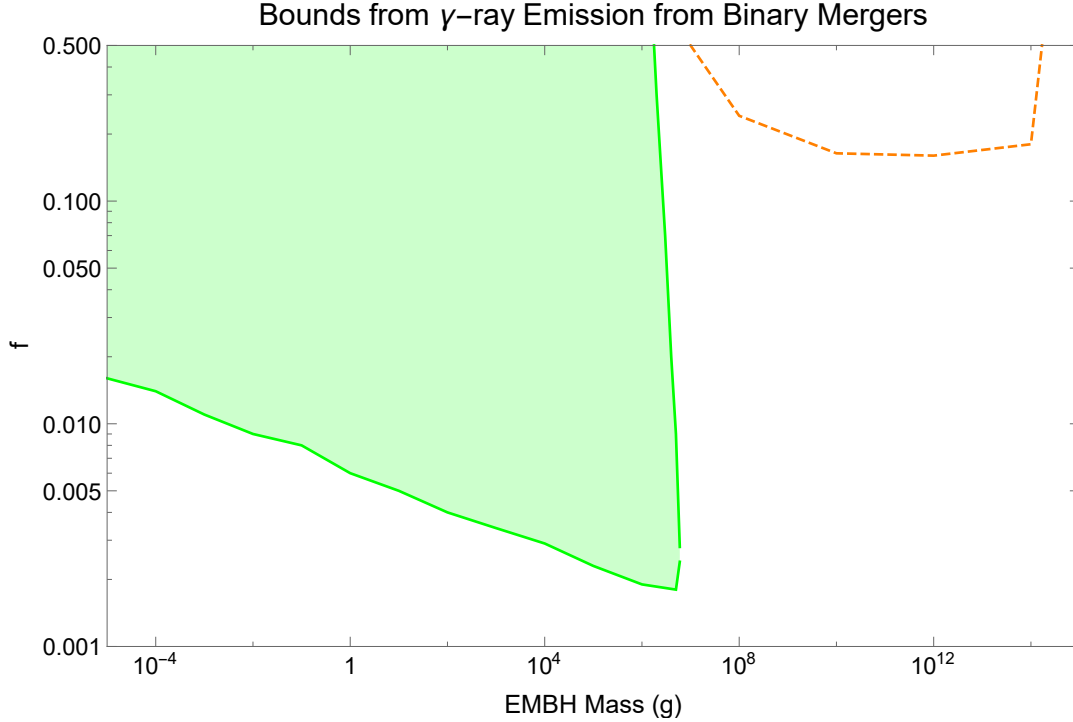


Figure 2: The region highlighted in green shows the bounds on EMBH abundance based on γ -ray emission from binary mergers. The green region focuses specifically on EMBHs that form binaries at a redshift where friction does not strongly influence the EMBH infall. The dotted orange line gives a rough estimate of the bounds that would arise from γ -ray emission from binary mergers where friction with the thermal bath changes binary infall dynamics, and reduces the number of mergers that happen by today. The friction-free bounds bend backward, weakening for high f for EMBH with masses between 10^6g and 10^7g . This happens because friction reduces the number of binaries that form and merge that can contribute to these bounds, in particular friction reduces the number of low eccentricity binaries that form. Increasing f decreases the distance between a binary and the next nearest EMBH, this decreases the typical eccentricity for binaries that form, which means a larger fraction of them are affected by friction. When friction effects begin to become important ($10^6 - 10^7\text{g}$) increasing f can weaken the bounds.

Reducing the typical eccentricity by increasing f means a larger fraction of binaries that would merge without friction instead get pulled apart and do not contribute to the bound.

Weaker bounds may be found by doing a separate analysis for heavy EMBHs ($> 10^7\text{g}$) that are sensitive to friction. These EMBHs will form bound pairs if they can traverse the distance separating them within one Hubble time, while infalling at a terminal velocity set by friction, their charge and their initial separation. Friction reduces the number of bound pairs that are able to form enough to make the constraint from γ -ray emission for EMBHs with $M > 10^7\text{g}$ weak compared to the other new constraints presented in this paper. For comparison we show a rough estimate of the constraint for EMBHs strongly affected by friction in Figure 2, but do not include this in our final set of constraints.

It has been suggested in [14] that fermionic radiation from near extremal magnetic black holes will be enhanced by a factor of Q , reducing the black hole lifetime by a factor of

$\frac{1}{Q}$, while keeping the surface temperature the same. We do not believe the presence or absence of this Q enhancement significantly changes the photon spectrum that ultimately reaches Earth for black holes with $M < 10^7 g$. The low energy portion of the spectrum comes from hadronic decays. If the surface temperature remains unchanged, the hadronic spectrum should have the same form, and decay down to a photon spectrum of the same form, so the low energy part of the spectrum is unchanged. Direct photons that then get reprocessed contribute to much of the high energy part of the overall photon spectrum. The Q enhancement may suppress the number of direct photons produced by a factor of $\frac{1}{Q}$ due to the reduction in the black hole lifetime. However, electrons and positrons, which would be produced at a Q enhanced rate, can replace the reduced photon radiation and produce a very similar signal with a peak shifted by $\mathcal{O}(1)$ relative to the usual direct photon peak [37]. Both the photon and electron spectra peak at energies well above E_{th} for all masses and z relevant to these bounds. The thermal bath reprocesses electrons and photons with $E > E_{th}$ in the same way [39]. As the vast majority of either signal will be reprocessed, we can safely assume the high energy signal that reaches Earth will be approximately the same whether it comes from direct photons or from direct electrons. Therefore the overall energy spectrum that reaches Earth should not change significantly if magnetically charged black holes decay to quarks and leptons at a Q enhanced rate.

3.4 Destruction of Large Scale Magnetic Fields

EMBHs can interact with and destroy large scale coherent magnetic fields. The bounds from this are subdominant to all other bounds derived in this paper, so we will only touch on them briefly.

Parker Bound There are multiple versions of the Parker Bound [40–42], a limit set on the abundance of magnetic monopoles based on their interaction with the early galactic magnetic field. The galactic magnetic field accelerates magnetic charges moving through it. The kinetic energy gained by the charges is removed from the field. Magnetic charges are constrained so that they do not destroy the Milky Way magnetic field or prevent it from forming. The protogalactic Parker bound offers the most stringent monopole abundance constraints of all the versions of the Parker bound [40]. It limits the monopole abundance during the collapse of the protogalaxy, when the galactic magnetic field was only a small seed field unsupported by a galactic dynamo. When applied to EMBHs this gives the bound

$$f < 0.06 \tag{3.20}$$

Stronger constraints, $f < 4 \times 10^{-4}$, and $f < 1.7 \times 10^{-3}$ were derived in [12] and [13] respectively by applying a Parker type bound to the Andromeda galaxy where the magnetic field is coherent over larger length scales than in the Milky Way. Uncertainty in this bound comes from uncertainty in the properties of the magnetic field in the Andromeda Galaxy [12]. We show the [12] bound in figure 3 for comparison to our other bounds.

Cluster Magnetic Fields The largest scale coherent magnetic fields observed in galaxy clusters are in radio relics which have magnetic fields coherent over $L \sim 2$ Mpc [43, 44]. EMBH in these galaxy clusters would form a diffuse magnetic plasma. This

plasma would suppress magnetic fields that extend over scales larger than its Debye length λ_d . A bound is derived from requiring that $\lambda_d > 2$ Mpc for an EMBH plasma in a typical galaxy cluster. This gives a bound on the EMBH abundance of

$$f < 0.7 \quad (3.21)$$

3.5 MACRO

MACRO was a dedicated monopole detector that ran from 1989 through 2000 [3]. The detectors and analyses are focused on dirac charge monopoles $g = g_D$ [3], however further analyses indicate that the detectors would have been equally or more sensitive to higher charge magnetic particles [45]. MACRO flux bounds should therefore be applicable to EMBHs.

The detectors relied on ionization effects from passing magnetic charges. Assuming EMBHs do not cause nucleon decays, which will be touched upon in section 4, then MACRO places an upper limit on the EMBH flux of [3]

$$F < 2.8 * 10^{-16} \text{cm}^{-2} \text{sr}^{-1} \text{s}^{-1} \quad (3.22)$$

This corresponds to a bound on f of

$$f < 217 \left(\frac{M}{g} \right) \quad (3.23)$$

4 The Effects of Proton Decay Catalysis on EMBH Bounds

As discussed in the introduction, it is reasonable to expect EMBHs to catalyze proton decay, perhaps analogous to the effect in monopoles from grand unified theories [10, 11]. However, due to the uncertainty of what can be at the 'core' of the EMBH (the strength of B-violation, the existence of short-distance hair, etc.), the cross section for this process may be model dependent.

We circumvent many of the complications and model dependencies associated with nucleon catalysis by looking for more robust bounds independent of the cross section for catalysis. Heat generated by catalysis can weaken the bounds from white dwarf destruction by generating convection currents that prevent the EMBHs from annihilating. On the other hand, catalysis can cause anomalous heating of neutron stars causing x-ray emission. In addition, the heating of white dwarfs can also set a (weaker) bound, while catalysis in the sun can be constrained by neutrino detectors such as Super Kamiokande. Magnetic monopole searches by the MACRO detector offer constraints for EMBHs at the lowest masses. These constraints are weakened, but still present when accounting for catalysis effects. No matter what the catalysis cross section is, we can place a robust bound below the dark matter abundance on the relic abundance of EMBHs at any mass.

We estimate the most robust bound by finding the threshold catalysis cross section needed to activate convection in white dwarfs, σ_{th} . This minimal cross section is then used to find bounds from white dwarf heating. Increasing the cross section above σ_{th} increases the heating in white dwarfs strengthening the heating bound. Reducing the cross

section below σ_{th} will allow EMBH annihilations to resume in white dwarfs, which gives a significantly stronger bound than heating effects can. For a set cross section, neutron star heating generates stronger bounds than white dwarf heating does. However, many different estimates of the catalysis cross section depend on the velocity of passing nuclei [46–48]. Nuclei move at very different velocities in white dwarf cores ($\sim 10^{-4}$) than they do in neutron star cores (~ 0.3), making it unreasonable to assume EMBHs with one specific cross section in a white dwarf will have the exact same cross section in a neutron star. In determining a robust cross section, we will only compare bounds that rely on catalysis in white dwarfs where we can give a more consistent description of the cross section. Catalysis bounds in the sun and in neutron stars will be described and shown for a specific cross section for comparison and for future reference for specific models of extremal magnetic black holes.

To find σ_{th} , we determine the minimal catalysis luminosity, L_{th} , needed to start convection in the white dwarf. This depends on the conditions in the white dwarf and is independent of the properties of the EMBHs inside of it. σ_{th} is the catalysis cross section for a given mass that would cause all EMBHs in the white dwarf core to radiate at a combined luminosity of L_{th} .

Whether the value of σ_{th} needed to start convection in white dwarfs is physically reasonable depends on two different length scales set by the EMBH and by the properties of the white dwarf core: a geometric scale, and a scattering length set by the medium. One might expect a catalysis cross section at the geometric scale where the magnetic field is larger in energy scale than the proton mass, where the dynamics are better described by two-dimensional degenerate radial fermions [14]. This cross section can be enhanced or severely suppressed due to the angular momentum barrier between the strong magnetic field of an EMBH and the electric charge and magnetic moment of an incoming nuclei [46]. This cross section will be referred to as the QCD cross section, σ_{QCD} going forward.

$$\sigma_{QCD} = \sqrt{\frac{\pi}{8}} \frac{M}{m_P \Lambda_{QCD}^2} \sim 2 \times 10^{-22} \text{cm}^2 \left(\frac{M}{g} \right) \quad (4.1)$$

where we define $\Lambda_{QCD} \equiv 218 \text{ MeV}$, the approximate QCD scale. All nuclei entering this region will have dynamics dominated by the background magnetic field and could plausibly have non-negligible overlap with a proton-decaying core.

While σ_{QCD} sets the region where nucleon decay may actually occur, the strong magnetic field around magnetic monopoles and EMBHs allows them to have even larger effective catalysis cross sections. For example, charged nuclei with non-zero magnetic moments accelerate and radiate photons when passing through the magnetic field near an EMBH, this can cause them to lose enough energy to fall into a bound magnetic state which brings the particle within σ_{QCD} [47, 48]. Any enhancement to the effective catalysis cross section, such as the one described here, is limited by scattering in the white dwarf medium. Nuclei falling toward the EMBH can scatter off of other nuclei and regain enough kinetic energy to escape before reaching the inner region where decay actually occurs. This introduces the second important length scale: the scattering length of the nuclei in the local medium. We

estimate the nuclei-nuclei scattering length in white dwarfs as

$$l_s = \frac{m_n}{\rho_{wd}} \frac{1}{\pi \lambda_d^2} \sim 5 \times 10^{-8} \left(\frac{T}{10^6 \text{K}} \right)^{-1} \text{ cm} \quad (4.2)$$

where m_n is the mass of the nuclei involved, λ_d is the Debye length in the white dwarf, and T is the temperature in the white dwarf. In principle, nuclei with non-zero magnetic moments will be attracted to the EMBH, and can fall in from distances larger than the scattering length. However, we find that the abundances of these nuclei (such as oxygen 17) in white dwarf cores are too small [49] to effect the bounds.

The length scales described above set upper limits on which values of σ_{th} , the minimal cross section needed to turn off annihilation in white dwarfs, are physically reasonable. Given that σ_{QCD} describes a region where nucleon decay may occur, any value of σ_{th} such that $\sigma_{th} \leq \sigma_{QCD}$ is physically plausible. Mechanisms exist to allow σ_{th} to grow larger than σ_{QCD} [47, 48], but this is limited by nuclear scattering, and thus we allow cross sections σ only up to this scale. Our 'physically plausible' condition is thus

$$\sigma \leq \sigma_M \equiv \text{Max}[\pi l_s^2, \sigma_{QCD}] \quad (4.3)$$

where we define σ_M as the maximal allowed catalysis cross section within the white dwarf core.

How we determine σ_{th} , the the EMBH annihilation rate, and the white dwarf heating bounds is elaborated on in the sections below. Figure 3 shows the robust bounds that emerge after determining the minimal catalysis cross section needed to start convection, along with other bounds that are not impacted by catalysis for a full view of the constraints available when catalysis is considered. Here we have made the simplifying assumption that once convection starts in a white dwarf, EMBHs will no longer annihilate. This is a conservative simplification. EMBHs may still reach each other and interact even while convection spreads them throughout the star. However determining the annihilation rate, as well as which particular catalysis cross sections generate a large enough temperature gradient in the core and strong enough convection to stop EMBH annihilation requires detailed modeling of convection in white dwarf cores. Such modeling is beyond the scope of this paper. A detailed consideration of how the EMBH annihilation rate evolves when catalysis and convection effects are considered will only yield more stringent bounds.

For illustration only, in Figure 4 we display all of the bounds that arise if we assume the catalysis cross section is fixed to be σ_{QCD} in all environments. Here additional bounds arise from physical processes such as neutron star heating and neutrinos from proton decay in the sun.

4.1 Convection in White Dwarfs

As explained in Section 3.2, EMBH abundances are strongly constrained by their ability to annihilate inside of white dwarfs and destroy them. Typical catalysis heating bounds are significantly weaker than those that arise from white dwarf destruction. However, when an EMBH falls into a white dwarf, or any medium, it can cause nearby nuclei to decay

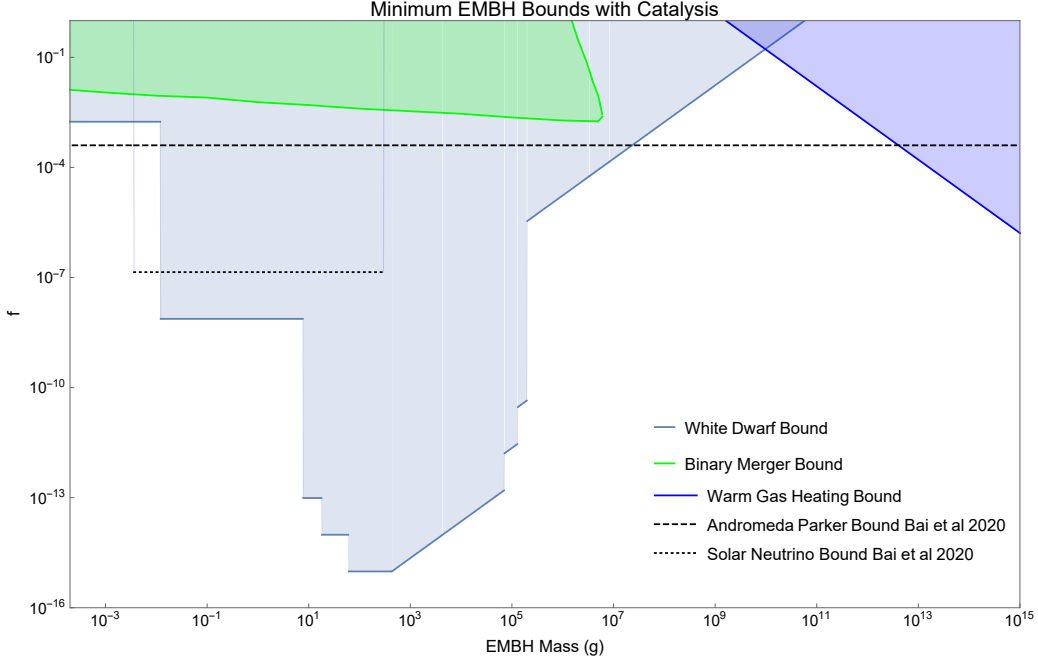


Figure 3: The colored regions denote the minimum bounds on the EMBH abundance with catalysis effects from white dwarfs considered. The overheating and annihilation bounds are related by catalysis effects and are thus combined in this plot and marked in light blue. The bounds from overheating or destroying $1 M_{\odot}$ white dwarfs were stronger than those for WD J0551+4135 for all EMBHs with masses above 0.012g. Lighter EMBHs cannot destroy a $1 M_{\odot}$ white dwarf when they annihilate so only WD J0551+4135 is used to derive constraints on EMBHs with $M < 0.012$ g. No physically reasonable catalysis cross section could prevent EMBHs with masses in the range $7 \text{ g} \lesssim M \lesssim 2 \times 10^5 \text{ g}$ from annihilating at all times in $1 M_{\odot}$ white dwarfs so the original annihilation bound remains in a somewhat weakened form. The bounds in this mass range appear as jagged step functions because the convection effects were considered at discrete cooling temperatures. If the convection effects were considered at all arbitrary cooling temperatures and times then the bound in this region would vary smoothly. There are physically plausible catalysis cross sections that prevent EMBHs outside of this mass range from annihilating inside of white dwarfs, and so bounds come from white dwarf heating instead. These bounds are shown assuming EMBHs have the minimum catalysis cross section needed to prevent annihilations. Bounds from gas heating and binary mergers are unaffected by catalysis and are described in sections 3.1 and 3.3 respectively. Constraints derived in the recent work [12] are shown in dashed and dotted lines for comparison, these will be labeled Bai et al 2020. The dashed line comes from a Parker bound set by the magnetic field in the Andromeda Galaxy. The dotted line comes from energetic neutrinos produced when EMBHs annihilate in the sun. We only show the latter bound for EMBHs with $M < 300 \text{ g}$ because heavier EMBHs get caught in the sun’s convection zone, suppressing their annihilation rate. We touch briefly on these constraints in sections 3.4 and 4.4

into lighter, more energetic particles. This releases the nucleon mass energy and makes EMBHs into sources of radiation. In a white dwarf’s core the energy radiated by this process can create a severe enough temperature gradient to initiate convection [50]. Friction between the EMBH and convecting material in the white dwarf drags EMBHs out of the center and spreads them throughout the convection region. This can prevent any EMBH

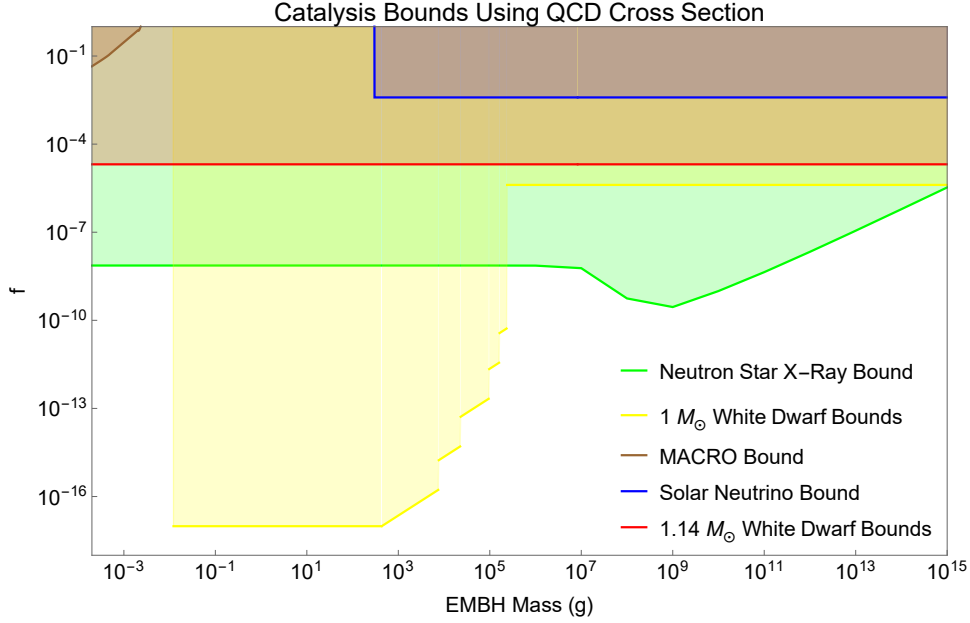


Figure 4: Catalysis bounds on EMBH abundance if we assume the catalysis cross section is σ_{QCD} . The yellow and red lines denote bounds from $1 M_{\odot}$ white dwarfs and WD J0551+4135 respectively. EMBHs with $M \lesssim 8000$ g do not produce enough heat through nucleon decays to turn on convection in $1 M_{\odot}$ white dwarfs, and the original annihilation bound stands. EMBHs with $8000 \text{ g} \lesssim M \lesssim 9 \times 10^5 \text{ g}$ will produce enough heat to stop annihilation at some times, but not all times in the $1 M_{\odot}$ white dwarf, and so the original annihilation bound remains, but in a weakened form. Heavier EMBHs will produce enough heat to turn on convection at all times. These are constrained due to the overheating of old white dwarfs (Section 4.2). EMBHs with catalysis cross sections equal to σ_{QCD} always produce enough energy to start convection in WD J0551+4135, so only heating bounds are displayed. The green region marks the constraint set by overheating old neutron stars. At masses below about 10^7 g the bound is weakened because EMBHs can annihilate inside of the neutron star reducing the number available to catalyse nucleon decay. The dip in this bound appears because only small number of EMBHs with masses above 10^7 g are needed to overheat a neutron star, so annihilation does not weaken the bounds in this mass range. This is elaborated upon in Section 4.3. The brown line in the upper left-hand corner marks constraints from a MACRO monopole search (Section 4.5). The blue line marks the EMBH abundance limit from Super Kamionkande observations of solar neutrinos. This bound cuts off for EMBHs with masses below 300 g because they easily sink to the stellar core and annihilate, reducing the number available to catalyze proton decay. Heavier EMBHs get caught in the solar convection zone and are much less likely to annihilate. This is described in Section 4.4.

annihilations from happening within 1 Gyr, eliminating the white dwarf annihilation bound. The catalysis cross section determines the amount of heat generated in the white dwarf core. This sets the temperature gradient, which determines whether convection takes place. If convection does not happen, then the conditions that determined the bound in section 3.2 stand with only minor modifications. Once convection starts, we assume the spreading of EMBHs throughout the white dwarf prevents annihilations. While annihilations can still happen once convection begins, including this effect requires detailed modeling of how EMBHs behave under specific convection conditions and how convective currents move

through the white dwarf, and would only yield stronger bounds than those presented here. To determine whether EMBH annihilations can happen in white dwarfs, we compared the minimum luminosity produced from EMBH induced nuclei decays needed to initiate convection, L_{th} , to L_m , the maximum luminosity that can be radiated by EMBHs in the white dwarf core assuming realistic catalysis cross sections and that enough are present in the star to annihilate under no catalysis conditions.

We determined L_{th} for a variety of white dwarf ages because younger white dwarfs are hotter, and can accommodate more EMBHs before convection turns on. This is elaborated on below.

This was done separately for both sets of white dwarfs used to find the original annihilation bounds, WD J0551+4135 and for CO white dwarfs with masses around $1 M_\odot$.

Throughout the conductive region of the white dwarf, the temperature gradient is

$$\left(\frac{dT}{dr}\right)_{cond} = \frac{-L_{tot}}{4\pi\kappa r^2} \quad (4.4)$$

where L_{tot} is the combined luminosity of all of the EMBHs in the white dwarf producing radiation through nuclear decays and κ is the conductivity of the white dwarf. We use the expression for κ presented in [30] for a white dwarf made of equal parts carbon and oxygen, with a density profiles for $1.14 M_\odot$ and $1 M_\odot$ white dwarfs derived from equations presented in Appendix D of [25].

Two conditions must be met for convection to occur, the first is that there exists a region in the star where the temperature gradient (4.4) is larger than the adiabatic temperature gradient which is defined as

$$\left(\frac{dT}{dr}\right)_{ad} = \frac{1}{4} \frac{T}{P} \frac{dP}{dr} \quad (4.5)$$

Where P is the pressure, which we estimate as $P = \int_r^{R_{wd}} \frac{dP}{dr'} dr'$. $\frac{dP}{dr} = \frac{GM_{int}(r)\rho_{wd}(r)}{r^2}$ is the pressure gradient, $M_{int}(r)$ is the mass contained within the radius r , $\rho_{wd}(r)$ is the mass density at r , these are found using density profiles for $1.14 M_\odot$ and $1 M_\odot$ white dwarfs derived using equations presented in [25]. The first condition to initiate convection is then

$$\left(\frac{dT}{dr}\right)_{ad} < \left(\frac{dT}{dr}\right)_{cond} \quad (4.6)$$

Starting with a surface temperature T_s , we calculate the temperature and $\frac{dT}{dr}$ as a function of r in km sized steps moving inward from the surface, and in m sized steps for the inner most kilometer of the white dwarf. At each step we check if the convective condition has been met. White dwarf interiors cool over time. This causes older white dwarfs to develop more extreme temperature gradients, causing convection to start at lower decay luminosities than in younger stars. Some EMBHs will start convection in cool Gyr-old white dwarfs but not within a hotter 100 Myr-old white dwarf. To account for this we considered the temperature gradient that would arise in white dwarfs at a variety of cooling ages Age= $\{10^9, 10^8, 10^7, 10^6, 10^5\}$ years, and their corresponding internal temperatures $T_s = \{10^{6.8}, 10^{7.3}, 10^{7.7}, 10^{7.85}, 10^{7.95}\}$ K respectively, as estimated in [31].

Assuming there is a region near the white dwarf core where the first condition for convection to happen (4.6) is met, we then check for the second condition needed to initiate convection. Buoyant forces acting on the white dwarf material must be greater than the viscous forces resisting deformation. The Rayleigh number Ra parameterizes the relationship between these forces. For spherical geometries Ra is [51]

$$Ra = \frac{4\pi G \rho_{wd}(r) D(r)}{3\chi\nu} r^5 \quad (4.7)$$

where $D(r)$ is the adiabatic excess at a given radius r [50]

$$D(r) = \frac{1}{T} \left[\left(\frac{dT}{dr} \right)_{cond} - \left(\frac{dT}{dr} \right)_{ad} \right] \quad (4.8)$$

and where χ is the thermometric conductivity, and ν is the kinematic viscosity [51], which we take from [52]. It has been determined in [53] that Ra must be greater than $\sim 10^3$ for convection to occur in a spherical system where heat is generated in the convection medium. If $Ra \lesssim 10^3$ in the entire region where ($D > 0$), then convection does not happen. The second condition for convection to happen is then that there exists a region in the white dwarf where

$$Ra \gtrsim 1000 \quad (4.9)$$

For each set of white dwarfs and for each cooling temperature, $T_s = \{10^{6.8}, 10^{7.3}, 10^{7.7}, 10^{7.85}, 10^{7.95}\}$ K, which correspond to typical white dwarf cooling temperatures at Age = $\{10^9, 10^8, 10^7, 10^6, 10^5\}$ years [31], we increased L_{tot} from 0 until the conditions needed for convection to occur, (4.6) and (4.9), are met. The minimum luminosity that allows these conditions to be satisfied in some part of the star is L_{th} . To determine if L_{th} is physically plausible for each temperature and mass we also calculated L_m the maximal luminosity that could be radiated from all of the accumulated EMBHs if they each had the maximum physically plausible cross section:

$$L_m = N_{acc} \rho_c \sigma_M v_n \quad (4.10)$$

Here N_{acc} is the number of EMBHs present in the white dwarf core, which we take to be the minimum number needed to destroy a white dwarf if catalysis did not happen, set by (3.13), v_n is the thermal velocity of an average nuclei in the white dwarf core, σ_M is the largest allowed cross section for the average nuclei in the white dwarf core. Only $L_{th} \leq L_m$ are physically plausible luminosities.

The original annihilation bounds remain unchanged if, at every temperature checked, the luminosity needed to start convection is more than the largest allowed catalysis luminosity, $L_{th} > L_m$. If $L_{th} > L_m$ at some temperatures and not at others, then the annihilation bound is modified so that the EMBH abundance is low enough to prevent white dwarfs from accumulating enough EMBHs for an annihilation to happen within the longest timescale at which $L_{th} < L_m$. Finally, if $L_{th} \leq L_m$ at every temperature scale checked, then there exists a physically reasonable catalysis cross section that prevents annihilation at all times.

To find this, we first determine the catalysis cross section, σ that corresponds to L_{th} for each mass and cooling age:

$$\sigma = \frac{L_{th}}{N_{acc}\rho_c v_n} \quad (4.11)$$

For a given mass, σ_{th} is the maximum of all of the different σ 's found for all of the different cooling temperatures considered. σ_{th} is determined separately for $1 M_\odot$ white dwarfs and for WD J0551+4135. The maximum of the two will be used to set the catalysis heating bounds in white dwarfs and will be referred to as σ_H . At low masses $M < 0.012$, where no annihilation bound exists for $1 M_\odot$ white dwarfs, σ_H is σ_{th} for WD J0551+4135. The calculated values of σ_{th} and σ_H can be found in Figure 5.

4.2 White Dwarf Heating

The heat produced from EMBH-catalyzed nucleon decays in white dwarfs older than a few billion years can be enough to keep these white dwarfs artificially hot.

White dwarfs older than a few billion years are expected to naturally cool to luminosities below $10^{-4}L_\odot$ [54], and in fact we observe old white dwarfs with luminosities below $10^{-4}L_\odot$ [55, 56], and lifetimes above 8 Gyr [27, 57, 58]. Constraints come from maintaining an EMBH abundance low enough to allow 8 Gyr old white dwarfs to cool below $10^{-4}L_\odot$. Constraints also come from keeping the EMBH abundance low enough that WD J0551+4135 is allowed to cool to its observed luminosity, $3 \times 10^{-4}L_\odot$ [26], within its estimated age of 1.3 Gyr [26].

The luminosity of EMBHs in a white dwarf core, L is given by

$$L = v_n \sigma_H \rho_c \quad (4.12)$$

with v_n as the thermal velocity of nuclei in the core $v_n = \sqrt{\frac{3T_{wd}}{m_n}}$, with $T_{wd} = 10^{6.5}\text{K}$, the temperature of a white dwarf with $L = 10^{-4}L_\odot$, and $T_{wd} = 10^{6.8}$ used for the internal temperature of WD J0551+4135, based on modeling in [31]. σ_H , was determined in the previous section, and is the smallest cross section that causes convection in both sets of white dwarfs across all times. The cross sections used for different EMBH masses are presented in Figure 5. While sources on catalysis in magnetic monopoles [46–48] suggest that the catalysis cross section can itself depend on the velocity of passing particles we note that all of these sources indicate that the cross section grows as the velocity decreases. If such a velocity dependence is present then σ_H for a young hot white dwarf, may correspond to a larger cross section in an older cooler one with lower thermal velocities. We choose to use σ_H in our estimate because the velocity dependencies are model dependent, the thermal velocities of nuclei in the hottest and coolest white dwarfs considered vary by less than an order of magnitude, and because accounting for velocity dependencies in the catalysis cross section will only cause it to grow and strengthen the heating constraint. Thus this bound is a bit conservative.

A white dwarf that has been allowed to accumulate EMBHs for t_{acc} years without annihilation will radiate with a combined luminosity

$$L_{cat} = L * \Gamma_{wd} * t_{acc} \quad (4.13)$$

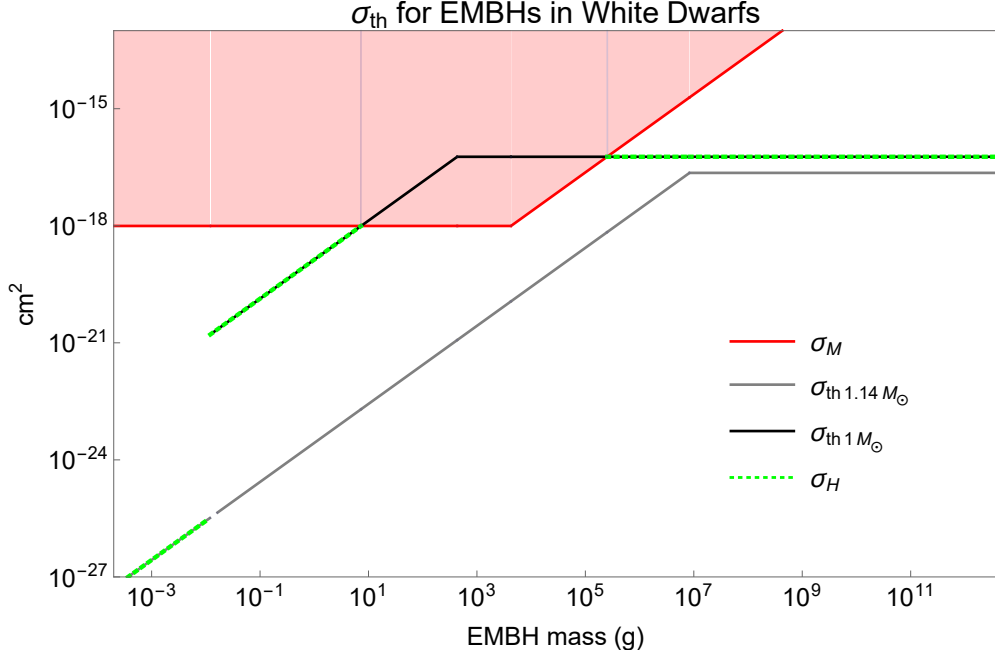


Figure 5: The above plot shows the minimal catalysis cross sections, σ_{th} , needed to just turn on convection at all white dwarf cooling times considered. The red line marks the upper limit on physically reasonable catalysis cross sections the white dwarfs, denoted σ_M . The σ_{th} that move above this line, into the region highlighted in red, are not physically feasible. The gray line marks σ_{th} found for the $1.14 M_\odot$ white dwarf WD J0551+4135. The black line marks σ_{th} found for the $1 M_\odot$ white dwarfs. σ_{th} for the $1 M_\odot$ white dwarfs crosses into the red region, indicating that within that mass range no physically viable catalysis cross sections turn on convection at all times, and that some form of the original annihilation bound stands. The heating bounds are set where the annihilation bound no longer stands, and are found using σ_H , marked with the green dotted line, which overlays parts of the black and gray lines. σ_H follows the smallest physically reasonable cross section that just turns on convection at all times in both sets of white dwarfs considered. σ_H follows $\sigma_{th,1.14M_\odot}$ at low masses where EMBH annihilation does not release enough energy to destroy a $1 M_\odot$ white dwarf. σ_H is not defined for EMBHs with $8 \text{ g} < M < 2 \times 10^5 \text{ g}$ where some form of the original annihilation bounds hold. The maximum feasible cross section, σ_M , depends on the temperature in the white dwarf. σ_{th} was ultimately set by the conditions in the white dwarfs at $T = 10^{7.95} \text{ K}$ which corresponds to a cooling time of 10^5 years, because this is when the star is hottest and least sensitive to energy injections from catalysis. Thus σ_M is plotted for $T = 10^{7.95} \text{ K}$. In WD J0551+4135 σ_{th} is always less than the scattering length, and thus always physically plausible.

Thus f is limited to keep L_{cat} below $10^{-4} L_\odot$ for $1 M_\odot$ white dwarfs older than $t_{acc} \sim 8 \text{ Gyr}$, and keep L_{cat} less than $3 \times 10^{-4} L_\odot$ for WD J0551+4135, assuming $t_{acc} \sim 1.3 \text{ Gyr}$. For WD J0551+4135 this age is a conservatively low estimate, as it is thought to result from the merger of two older white dwarfs (1.3 Gyr ago) that would themselves have had more time to accumulate EMBHs [26]. The bounds on EMBH abundances from white dwarf heating can be found in Figure 3.

4.3 Neutron Star Heating and Background X-Rays

The effects of magnetic monopoles falling into neutron stars was explored thoroughly in [59]. Once a monopole has fallen into the neutron star, neutrons will interact with the monopole, decay via catalysis, and release their mass energy into lighter particles. The power radiated by all of the monopole catalyzed decays will heat the neutron star, increasing its x-ray radiation. Constraints come from limiting the diffuse x-ray signal to be below that of the observed soft x-ray background. This same analysis can be applied to EMBHs.

This picture is complicated by annihilation effects, and the potential type II superconducting core of neutron stars. Annihilation of EMBHs will reduce the active number in the star (and not blow up the star) and thus reduce the x-ray signal. However, a type II core will prevent EMBH annihilation, whereas a different core, one that transitions to a type I superconductor or to an exotic state of matter may offer little resistance to annihilation. This uncertainty will be discussed below.

The neutron star must first capture a passing EMBH. The escape velocity is about $\sim 0.3c$. An EMBH entering the neutron star at these velocities will lose energy due to friction with the electron fermi gas in the neutron star [60]. We estimate the neutron star stopping power using (3.6) above, where now $E_f \sim 100$ MeV is the electron fermi energy, $n_e \sim 10^{36} \text{cm}^{-3}$ is the electron density inside of a neutron star, and v is the velocity of the infalling EMBH [61]. Numerically we find that a neutron star with 10 km radius will be able to capture the entire relevant mass range of EMBHs.

Once inside of the neutron star, an EMBH will begin radiating with a luminosity L_{ns} that can be found using

$$L_{ns} = 2.5 \times 10^{24} \frac{\sigma_{cat}}{\text{bn}} \left(\frac{v_{ns}}{0.3} \right) \left(\frac{\rho_{ns}}{5 \times 10^{14} \text{g cm}^{-3}} \right) \text{GeV s}^{-1} \quad (4.14)$$

Where we have used 0.3 for the neutron velocity, a number density set by the mass density $\rho_{ns} \sim 5 \times 10^{14} \text{g}$, and the cross section σ_{cat} . For illustrative purposes we will show the behavior of this bound if $\sigma_{cat} = \sigma_{\text{QCD}}$ in neutron stars.

When annihilation effects are not relevant, all of the EMBH accumulated in a neutron star will have a combined luminosity of $L_{tot} = N_{acc} L_{ns}$ where N_{acc} is the total number of EMBH in the neutron star. When annihilation is fast compared to the accumulation rate the expected number of EMBHs that actually remain in the neutron star all carry the same sign charge and is set by a random walk with N_{acc} steps. In this case $L_{tot} = \sqrt{N_{acc}} L_{ns}$. We take $N_{acc} = t_{ns} \Gamma_{ns}$, where t_{ns} is the age of the neutron star, and using a radius $r_{ns} = 10$ km and an escape velocity $v_{esc} = 0.3$, the rate Γ_{ns} is

$$\Gamma_{ns} \approx \left(\frac{\rho_{dm} f}{M} \right) \pi r_{ns}^2 \frac{v_{esc}^2}{v} \sim 5 f \left(\frac{m}{g} \right)^{-1} \text{s}^{-1} = 1.4 \times 10^{17} f \left(\frac{m}{g} \right)^{-1} \text{Gyr}^{-1} \quad (4.15)$$

The energy output from all of the EMBHs in a neutron star will give it a surface temperature of

$$T_{ns} = \left(\frac{L_{tot}}{4\pi r_{ns}^2 \sigma_b} \right) \quad (4.16)$$

where σ_b is the Stefan-Boltzmann constant.

4.3.1 Bounds from Overheating Neutron Stars

The bounds on EMBH abundance come from limiting the amount of x-ray radiation coming from catalysis heated neutron stars. We follow the analysis done in [59].

A neutron star heated to a temperature T_{ns} by catalysis would radiate like a black body with a differential luminosity of [59]

$$\frac{dL}{dE} = 2 \times 10^{36} \left(\frac{r_{ns}}{10 \text{ km}} \right)^2 \frac{E^3}{e^{E/T} - 1} \text{ ergs KeV}^{-4} \text{ s}^{-1} \quad (4.17)$$

The differential flux that reaches earth is

$$\frac{dF}{dE} = \frac{dL}{dE} \frac{e^{-\tau(l,E)}}{4\pi l^2} \quad (4.18)$$

Where l is the distance to the neutron star and $\tau(l, E)$ is the absorption length of photons with energy E within the galaxy and is described in more detail below.

The catalysis luminosity of an individual neutron star depends on the number of EMBHs it has accumulated, which depends on its age. To get the total flux from all of the neutron stars contributing to the total x-ray flux, one must integrate over all of the unique luminosities as a function of age over the range of possible ages of the neutron stars. For simplicity, we assume neutron stars in the galaxy are produced at a constant rate over $\sim 10^{10}$ years, and have a local number density of $n_{ns} \sim 10^{-4} \text{ pc}^{-3}$ [59]. As we will explain in Section 4.3.2 EMBHs may be free to annihilate in up to 90% of neutron stars. Therefore when calculating the total radiation from nearby neutron stars, we will assume $n_* \sim 10^{-5} \text{ pc}^{-3}$ accumulate EMBHs at a rate $\propto t_{ns}$, and $n_* \sim 10^{-4} \text{ pc}^{-3}$ accumulate EMBHs at a rate $\propto \sqrt{t_{ns}}$.

Accounting for absorption in the ISM, the total differential flux from all of the neutron stars out to a distance of $R^* \sim \text{few kpc}$, about as far as the x-ray signal is expected to be able to travel without scattering [59], is

$$\frac{dF}{dE_{tot}} = \frac{n_* B(E)}{n_0 \sigma_{abs} t_0} \int_0^{t_0} \frac{dL}{dE} dt_{ns} \quad (4.19)$$

where t_{ns} is the age of the neutron star, t_0 is 10 Gyr, and $B(E)$ is the integrated fraction of photons with energy E from all neutron stars within a few kpc of earth. The full analytical form of $B(E)$ and τ can be found in [59].

The resulting flux that reaches Earth will be compared against sounding rocket soft x-ray observations done by McCammon et al [62]. The counting rate per frequency band, Γ_{band} for a given flux is

$$\Gamma_{band} = \int \frac{dF}{dE_{tot}} A_{band}(E) dE \quad (4.20)$$

where $A_{band}(E)$ is the detector response function for each of the four different x-ray detection bands considered in [59]. $A_{band}(E)$ can be found in Table 1 of [59].

In large regions of the sky the counting rate measured by [62] was $\frac{1}{3}$ the all sky average [59]. As in [59] we set limits by comparing the count rate of soft x-rays produced from radiating neutron stars, to $\frac{1}{3}$ the all sky average measured by [62]. We use the weakest of the limits derived from the four bands as the final limit on f .

The constraints derived are shown in Figure 4.

4.3.2 Annihilation Effects and the Superconducting Core

Whether EMBHs can annihilate in a neutron star depends on the properties of its inner core.

The inner 5-8km of a neutron star are thought to be occupied by a type II superconductor [63]. When an EMBH falls into a neutron star, it sinks into the superconducting surface. The superconductor produces 2 flux tubes around the EMBH for each unit of dirac magnetic charge $q_d = \frac{1}{2e}$ it carries. Each flux tube carries a magnetic flux of $\frac{\pi}{e}$, and an energy of $\sim 2 \times 10^{11} \text{ GeV cm}^{-1}$ [64]. This energy per unit length of flux tube can be treated as a tension connecting the EMBH back to the surface of the superconducting core.

EMBHs will sink to where gravitational force from the neutron star and tension force from lengthening the flux tubes balance, and form a surface of suspended EMBHs. This happens $\sim 0.6 \text{ km}$ above the center of the neutron star independent of the EMBH mass. In agreement with [12], we find that annihilation between suspended EMBHs is too slow to alter the radiation bounds if the neutron star remains a type II superconductor at the EMBH surface. Neutron stars are poorly understood at these depths. They may transition to a type I superconductor [65, 66] or to exotic states of matter [67]. Neither of which are expected to support the EMBH surface or prevent EMBHs from falling to the core and annihilating. This would severely weaken the bounds, by reducing the number of EMBHs available in the neutron star to catalyze neutron decay.

Neutron star cores require densities above $\sim 7 \times 10^{14} \text{ g cm}^{-3}$ to transition to a type I superconductor or other exotic state [65]. While the equation of state in neutron star cores and the particular mass range for neutron stars that avoid exotic transitions in their inner core remains an area of active research [67], lighter neutron stars are expected to have less dense cores, and are not thought to transition [68]. Based on modeling of low mass neutron stars done in [69], we estimate that neutron stars with masses $\lesssim 1.1M_\odot$ can safely be treated as having a core with a density below the transition threshold. Based on the available mass measurements for neutron stars [70] we estimate that $\sim 10\%$ have masses below $\sim 1.1M_\odot$. This 10% of neutron stars which do not permit EMBH annihilation will keep the vast majority of EMBHs they accumulate. The remaining 90% of neutron stars, those that may allow EMBHs to annihilate, will only be able to amass EMBH at a random walk rate proportional to the square root of the number of EMBHs that pass through it. We make the conservative assumption here that annihilation is fast in any neutron star where annihilation could be possible, as this gives the lowest estimate for the total number of EMBHs accumulated in neutron stars, which gives the lowest neutron star x-ray luminosity and the weakest bounds.

At high masses ($M \gtrsim 10^9 \text{ g}$) a single EMBH can cause a neutron star to overheat, so annihilation suppression no longer matters. At masses between 10^7 g and 10^9 g , neutron stars accumulate a few EMBHs, so N_{acc} is not so much smaller than $\sqrt{N_{acc}}$ and all neutron stars contribute to the bound. The bound on EMBHs with masses below 10^7 g is dominated by radiation from non-annihilating neutron stars.

4.4 Proton Decay in the Sun, Neutrinos and SuperK

Proton decay in the sun has been constrained by neutrino observations at Super Kamiokande [71]. Most of the range of masses of EMBHs that we focus on will become trapped in the sun when passing through, and cause proton decay once inside the sun. Heavier ones will get caught in the convection zone, while those lighter than about 300 g will make it to the core and eventually annihilate. Bounds will come from the steady-state number of EMBHs in the sun. These bounds are weaker than those derived for neutron stars and white dwarfs when the catalysis cross section is held constant. However, some enhancements to the cross section from the existence of EMBH-proton bound states [47, 48], or due to angular momentum effects [46] can lead the solar neutrino bound to become stronger than the white dwarf heating bound for some masses. Details of this constraint are included for reference when considering specific EMBH models with specific σ_{cat} . As a toy example we will assume $\sigma_{cat} = \sigma_{QCD}$ for the remainder of this section. We also note that [12] derives stronger solar bounds by considering neutrino emission from EMBHs that annihilate in the solar core. These bounds should apply to EMBHs light enough to sink to the stellar core and annihilate; however, [12] does not consider how EMBHs with masses above 300 g can get trapped in the convection zone which suppresses the EMBH annihilation rate and weakens these specific constraints on EMBH abundance.

Super Kamiokande is a water Cherenkov detector sensitive to neutrinos above 5.5 MeV [72]. About half of proton decays produce charged pions, which themselves dominantly decay into three neutrinos with energies in the 10's of MeV [71] via $\pi^+ \rightarrow \mu^+ + \nu_\mu \rightarrow e^+ + \nu_e + \bar{\nu}_\mu + \nu_\mu$. The analysis done in [71] limits the flux of neutrinos resulting from proton catalysis in the sun with 90% certainty to $I_{90} < 166.6 \text{ cm}^{-2} \text{ s}^{-1}$. This limits the proton decay rate in the sun to be less than f_p^{max} where

$$f_p^{max} = \frac{4\pi d^2 I_{90}}{f_{\pi^+}(1 - a_{\pi^+})} = 4 \times 10^{29} \text{ s}^{-1} \quad (4.21)$$

where $f_{\pi^+} \sim 0.5$ is the branching fraction of protons into π^+ + anything, $a_{\pi^+} \sim 0.2$ is the probability that a pion get absorbed by the solar core [71], and d is the Earth-sun distance.

The sun is a large ball of plasma. An EMBH passing through it will lose energy as described in eqn (3.1). Since the average galactic velocity of these black holes is $v \simeq 10^{-3}$ and the solar escape velocity from the surface is $v_{esc} \simeq 2 \times 10^{-3}$, the EMBH needs to lose an order one fraction of its kinetic energy to become gravitationally bound to the sun. Taking an average internal temperature for the sun of $T = 2 \times 10^6 K$ in (3.1), one finds an order one energy loss for EMBH masses of $M \gtrsim 0.5 \text{ g}$.

Next, we need the sun's rate of accumulation of EMBHs with $M > 0.5 \text{ g}$. The sun accumulates them at the (slightly) Sommerfeld enhanced rate of

$$\Gamma_\odot \sim \pi r_\odot^2 \left(\frac{\rho_{DM} f}{M} \right) \left(1 + \frac{v_{esc}^2}{v^2} \right) v = 4 \times 10^{22} \text{ Gyr}^{-1} f \left(\frac{M}{\text{g}} \right)^{-1} \quad (4.22)$$

where $r_\odot \simeq 7 \times 10^5 \text{ km}$ is the solar radius.

Heavier EMBHs will get trapped in the convection zone, which makes up the outer third of the sun. Here the temperature varies from 2×10^6 K at the base of the convective zone to 5700 K at the surface. The convective motions have velocities of about 10^{-6} [73].

Using the solar mass profile $M_\odot(x)$ [74], we add the term $G_N M M_\odot(x)/(r_\odot - x)^2$ to Equation (3.1) to account for the change in gravitational potential and numerically integrate the energy loss as the EMBH traverses the sun. We look for values of M for which the velocity drops below the convection velocity and find this occurs if $M \gtrsim 300$ g. Thus this range of masses will be trapped in the convection region.

One can check that annihilation within the convection region is unimportant. EMBHs trapped in the convection region will move with stellar convection currents and will annihilate at a rate $\Gamma \sim N_{acc} n_{acc} \sigma v_{th}$ where here, N_{acc} and n_{acc} are the number and number density of EMBH accumulated in the convection region, v_{th} is the thermal velocity, and σ is a cross section defined by the region where two EMBHs approaching at free fall velocity can reach each other within the time a convection flow would cross the convection region $\sim \frac{2 \times 10^5 \text{ km}}{3 \times 10^{-1} \text{ km s}^{-1}} \sim 7 \times 10^5 \text{ s}$ (a rough 'coherence' time for the flow). Γ is never large enough to significantly alter the number of EMBHs accumulated in the sun, so we neglect its contribution to these constraints.

The proton catalysis rate is

$$f_p = \Gamma_\odot t_\odot n_p v_p \sigma_{cat} \quad (4.23)$$

where $t_\odot = 4.6$ Gyr is the age of the sun, n_p is the proton number density set by the local density 0.2 g cm^{-3} , $v_p \sim 10^{-4}$ is the local proton thermal velocity, and σ_{cat} is catalysis cross section. For illustrative purposes we will set $\sigma_{cat} = \sigma_{QCD}$. Comparing this with this rate with the current bound (4.21) gives our constraint for masses $M > 300$ g.

4.4.1 Annihilation in the Sun

EMBHs with $M < 300$ g pass through the convection region, and are free to sink to the core. The local field at the bottom of the convection region, estimated to be at most 100 Gauss [75], will not be able to stop EMBH passage into the core.

The vast majority of EMBHs that sink to the core will ultimately annihilate. Only EMBHs that have not yet annihilated can contribute to proton catalysis. The total number of EMBHs in the sun at any one time N_{tot} , is made up of those that have not yet annihilated for one of two reasons – either they are in the process of sinking to the core (N_{sink}), or they are part of a charge imbalance at the core due to the random walk of charge accumulation (N_{ran}). There could additionally be a delay in annihilation if there is a strong enough magnetic field in the core of the sun, but we will ignore this possibility to set a conservative bound (the bound becomes stronger if they are kept from annihilating). Thus $N_{tot} = N_{sink} + N_{rand}$.

We can estimate the number of black holes in transit via:

$$N_{sink} = \Gamma_\odot t_{sink} \quad (4.24)$$

where the sinking time t_{sink} can be computed numerically. Using estimated temperature and density profiles in the sun [74], we find to a good approximation

$$t_{sink} \sim 10^3 s \left(\frac{M}{g} \right) \quad (4.25)$$

for masses above 0.5 g. Thus, for these masses, the number of black holes in transit is $N_{sink} \sim 10^9 f$.

On the other hand, N_{rand} is accumulated as a random walk, from random asymmetries in the signs of the EMBHs passing through the sun over its lifetime t_{\odot}

$$N_{rand} = \sqrt{\Gamma_{\odot} t_{\odot}} \simeq 4 \times 10^{11} \sqrt{f} \left(\frac{M}{1 \text{ g}} \right)^{-\frac{1}{2}} \quad (4.26)$$

The EMBHs that are sinking toward the core, and those in the innermost region of the star are sitting in slightly different environments and will have different catalysis rates. We estimate the outer core where EMBHs are sinking to have a $T_{out} \sim 7 \times 10^6$ K, and $\rho_{out} \sim 50$ g cm⁻³, and the inner core where the random walk EMBHs reside to have $T_{in} \sim 16 \times 10^6$ K and $\rho_{in} \sim 150$ g cm⁻³.

One can find the catalysis rates for sinking EMBHs, f_{sink} and for random walk EMBH, f_{rand} , by putting N_{sink} and N_{rand} into equation 4.23 with the appropriate temperatures and proton densities. The total catalysis rate is the sum of these two rates. $f_p = f_{sink} + f_{rand}$. This must be less than f_p^{max} given by Super K. The Super K bounds on the EMBH abundance using σ_{QCD} are shown in the Figure 4.

One might worry that the accumulated random walk magnetic charge might change the behavior of the sun. The maximum random walk charge possible for EMBHs that make it to the stellar core, would produce a magnetic field $\sim 10^{-6}$ G in the lower convection region where the local magnetic field influences solar dynamics, about 200,000 km from the stellar core. The magnetic field in the lower convection region could be as high as 100 G [75], indicating that the magnetic charge from EMBHs accumulating in the sun should not alter stellar dynamics.

4.5 Direct Constraints

The magnetic monopole detector MACRO, described in Section 3.5, is sensitive to nucleon decay effects. Nuclear catalysis from a traversing monopole produces extra radiation which changes the sensitivity of MACRO's detectors and requires a separate analysis. MACRO has produced separate analyses and flux bounds for monopoles that do not catalyze nucleon decay [3], and for those that do [76].

In the catalysis case, the flux limit from MACRO data depends on the catalysis cross section. Calculations of the flux limit as a function of the catalysis cross section for a magnetic charge moving at $v \sim 10^{-3}$, $F(\sigma_{cat})$, are presented in Fig 10. of [76]. Increasing the catalysis cross section weakens MACRO's ability to verify EMBH events [76]. Flux limits are only calculated for EMBHs with catalysis cross sections up to $\sigma_{cat} = 10^{-24}$ cm². We take this cross section and the corresponding flux limit $F \lesssim 10^{-15}$ cm⁻² s⁻¹ sr⁻¹, as it is the most conservative limit considered in [76]. This gives the constraint.

$$775 < \left(\frac{m}{g}\right)^{-1} f \quad (4.27)$$

This and all of the combined catalysis constraints can be seen in Figure 4.

5 Non-Extremal Magnetic Black Holes

Some of the constraints on EMBHs also apply to non-extremal magnetic black holes. If the Q enhancement to the radiation rate of leptons and fermions described in [14] is present then sub-extremal magnetic black holes only survive until present day if they have a mass of at least $\gtrsim 10^{17}g$, as this makes their surface temperature too low to effectively radiate electrons and positrons [14]. These heavier sub-extremal black holes are constrained by their interactions with warm ionized gas in the Milky Way, described in Section 3.1, and by their interactions with white dwarfs. We also note that some of these heavy black holes can cause neutron stars to collapse into black holes. We define the fractional charge of a sub-extremal black hole, q as

$$q \equiv \frac{Q}{Q_{ext}} = \frac{Qm_P}{M} \quad (5.1)$$

Where Q_{ext} is the extremal charge of a black hole with mass M .

5.1 Gas Heating

The constraints derived in Section 3.1 adjusted to account for sub-extremal black holes become:

$$q^2 f < 3 \left(\frac{M}{10^9 g} \right)^{-1} \quad (5.2)$$

This bound can be extended up to very high mass charged black holes. The bound is cut off when charged black holes do not pass through warm ionized clouds regularly enough to alter their behavior. The bound also cuts off when charged black holes lose a significant fraction of their kinetic energy from passing through warm ionized gas clouds. For very heavy EMBHs and charged black holes, those with masses above $\sim 10^{21}g$, a single black hole passing through a warm gas cloud may deposit the total amount of energy needed to overheat the entire cloud. This large amount of energy is not initially deposited throughout the entire cloud, but into a smaller region defined by the plasma attenuation length $l \sim 16$ km as described in (3.1). If all of the energy needed to heat a ~ 2 pc cloud is deposited into a cylindrical cross section of the cloud with a radius of about 16 km, the heated region will reach extreme temperatures causing it to expand supersonically until it cools significantly. While this may not evenly heat the entire cloud, it would significantly alter its structure and behavior within a time comparable to the sound crossing time, which is $\sim 5 \times 10^5$ yr for typical warm clouds [22].

The ISM is actively evolving. Regions occupied by warm ionized medium may cool to become cool neutral medium or be heated by supernova shocks to become hot ionized

medium. These phase changes happen on time scales of 10^6 yr [22]. We limit the abundance of charged black holes with masses above 3×10^{21} g, so that typically warm ionized clouds encounter a magnetically charged black hole less often than once per 10^5 yr. The cutoff excludes charged black holes that could pass through a cloud often enough to disrupt it faster than less exotic processes should be able to change the phase of the cloud.

This bound is also cut off when charged black holes lose $\mathcal{O}(1)$ of their kinetic energy due to friction with the warm ionized medium over ~ 10 Gyr. Charged black holes that lose this much kinetic energy or more will not be able to maintain their orbits in the Milky Way and will sink toward the galactic center. There may be interesting phenomenology around charged black holes that sink toward the galactic center, but we have not found new constraints that arise from this behavior.

Modifying (3.2) for a sub extremal magnetic black hole gives

$$\frac{dE}{dt} = 9 \times 10^{-3} q^2 \left(\frac{M}{10^9 \text{ g}} \right)^2 \text{ erg s}^{-1} \quad (5.3)$$

for EMBHs passing through warm ionized regions. The Warm Ionized Medium (WIM) fills about 1% of the galactic disk [77]. Charged black holes lose energy most efficiently in the WIM, so we will neglect energy loss from gas in other phases of the ISM. Most dark matter in the galaxy $\sim 90\%$ sits outside of the galactic disk in the dark matter halo. We assume then that black holes moving along virial orbits around the galactic center spend $\sim 10\%$ of their time in the galactic disk. Considering these properties of dark matter and the ISM, we estimate that charged black holes will lose $\mathcal{O}(1)$ of their kinetic energy in 10 Gyr if

$$\left(\frac{M}{10^{19} \text{ g}} \right) q^2 \gtrsim 1.6 \quad (5.4)$$

We cut off the gas heating bound where this is saturated.

The bounds for EMBHs of different masses and extremality fractions q are shown in Figure 6

5.2 White Dwarf Consumption

Separate constraints arise from how these black holes interact with white dwarfs. Black holes with masses above 10^{17} g can easily consume a $1.2M_\odot$ white dwarf they fall into within ~ 1 Gyr. The abundance of magnetically charged black holes with masses above 10^{17} g is constrained by the existence of hundreds of white dwarfs older than a Gyr and with masses above $1.2M_\odot$ [27]. We use white dwarfs in this mass range because their higher density allows them to exert stronger frictional forces on magnetic black holes than lighter white dwarfs do. They ultimately yield stronger bounds. While uncharged black holes might not get caught inside of a white dwarf long enough to consume it, the large frictional forces the fermi gas inside a white dwarf exert on a magnetic black hole may be sufficient to trap it.

The friction a sub-extremal black hole will experience when falling into a white dwarf can be found simply by modifying equations (3.6) and (3.1) to accommodate a black hole

with sub-extremal charge. This gives

$$\frac{dE}{dx} = \frac{Ge^2\sqrt{2m_e}M^2q^2}{\pi^2} \text{Log} \left[\frac{2E_f}{\nu_\sigma^{ei}} \right] \times \int_{-1}^1 \int_{-1}^1 \int_0^\infty \sqrt{E_e} \times f(E_e) (1 - f(E_e + dT)) dx dy dE_e \quad (5.5)$$

and

$$\left(\frac{dE}{dx} \right)_f = - \frac{16\pi^{1/2}Ge^2n_e}{3\sqrt{2Tm_e}} M^2 q^2 v \left[\ln(4\pi n_e L_D^2 l) + \frac{2}{3} \right] \quad (5.6)$$

Using this and the $1.2M_\odot$ white dwarf density profiles derived from [78] we numerically solve for the minimal extremality fraction, q , black holes of mass M require to get trapped inside of a white dwarf. We found that a black hole of mass M requires

$$q \gtrsim 3 \times 10^{-16} \left(\frac{M}{10^{17}\text{g}} \right)^{-1/2} \quad (5.7)$$

to get caught in a white dwarf. All black holes with q above this threshold will get caught in a $1.2M_\odot$ white dwarf.

Estimates in [25] indicate that an uncharged black hole residing inside of a white dwarf should be able to consume the entire white dwarf within a time

$$\tau \sim \frac{c_s^3 m_P^4}{4\pi\lambda\rho_{wd}} \left(\frac{1}{M} - \frac{1}{m_{WD}} \right) \sim 32 \text{ Myr} \frac{10^{17}\text{g}}{M} \quad (5.8)$$

where $c_s \sim 3 \times 10^{-2}$ is the speed of sound in a $1.2M_\odot$ white dwarf, λ is an order 1 constant, $\rho_{wd} \sim 10^8 \text{g cm}^{-3}$ is the density at the core of a $1.2M_\odot$ white dwarf, and m_{WD} is the mass of the consumed white dwarf [25]. One might worry that magnetically charged black holes do not accumulate mass at the same rate as uncharged black holes due to complications with the magnetic field or because absorbing electrically charged matter will make the black hole super extremal. The strong magnetic field around a charged black hole will classically cause infalling charged particles to move along conic geodesics and can repel charged particles before they reach the event horizon [79]. The magnetic field of the black hole cannot change the velocity of infalling matter, so in the most extreme case of magnetic repulsion, material originally infalling at the sound speed c_s could become material outflowing at the sound speed. The pressure from $\rho_{wd} \sim 10^8 \text{g cm}^{-3}$ of material moving away from the black hole at c_s is approximately four times greater than the ambient pressure in the core of the white dwarf. The density of material around the accreting black hole would be reduced until the pressure of outflowing material equals the pressure in the surrounding area. This happens when ρ_{wd} is reduced by a factor of ~ 4 in the area around the black hole. This would increase the accretion time by up to a factor of ~ 4 . Even with this increase in the accretion time, all black holes with masses above 10^{17}g will still be able to consume an entire $1.2M_\odot$ white dwarf within a Gyr. EMBHs in this mass range are heavy enough that they will not become super extremal upon absorbing an electron or a charged nuclei because the magnetic and electric charges add in quadrature. A black hole that gains electric charge will also quickly neutralize as it will become more attractive to particles of the opposite charge.

The constraint comes from limiting the magnetic black hole abundance so that $1.2M_\odot$ white dwarfs do not accumulate 1 magnetic black hole capable of consuming it within its

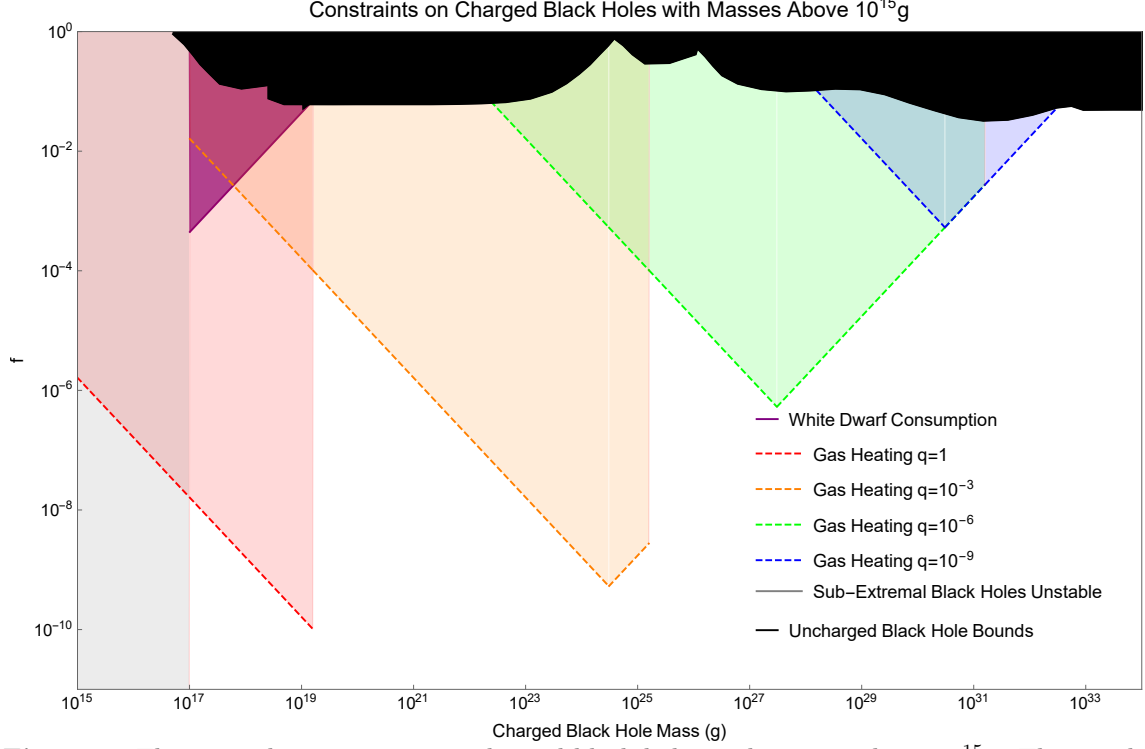


Figure 6: These are the constraints on charged black holes with masses above 10^{15} g. The purple region is excluded by white dwarf consumption. This bound applies to all magnetically charged black holes with a charge that satisfies (5.7). The dashed lines represent bounds that come from heating warm ionized clouds in the Milky Way. Each color is the bound for black holes that carry a different fraction q of the full extremal charge. The gas heating bound tilts upward when f becomes small enough that only one black hole passes through a typical warm gas cloud every 10^5 years. The gas heating bound cuts off entirely when charged black holes would lose more than $\mathcal{O}(1)$ of their kinetic energy due to interactions with the warm gas clouds over a period of 10 Gyr. The gray shaded region marks black holes with masses below 10^{17} g, which is the minimum mass needed for a sub extremal black hole to be stable over cosmological timescales [14]. Only extremal black holes are stable in the gray region. Already existing bounds on uncharged black holes that apply to charged black holes are marked in black (from [80]).

first Gyr of life. This gives the constraint.

$$f < 10^{-4} \left(\frac{M}{10^{17} \text{g}} \right) \quad (5.9)$$

for all magnetic black holes with q that satisfies (5.7).

The constraints for black holes with masses above 10^{15} g are shown in figure 6

5.3 Neutron Star Collapse

The recent LIGO observation of a $2.6 M_{\odot}$ object occupying the "mass-gap" between the theoretical upper mass for neutron star and lower mass for stellar black holes [81] has raised questions about how such a compact object could form. It has been suggested that a low mass black hole, perhaps the object observed by LIGO could result from a neutron

absorbing non-annihilating dark matter and collapsing into a black hole [82]. Some magnetic black holes would be able to cause this collapse because the friction between them and the electron Fermi gas in the neutron star allows them to be captured by the neutron star, while uncharged primordial black holes are much less likely to get trapped in a neutron star they pass through.

The minimum accretion rate for a black hole in a degenerate neutron gas with a stiff equation of state, as one might expect in a neutron star core was found in [83] to be:

$$\dot{M} = 3 \times 10^4 \left(\frac{M_\odot}{s} \right) \frac{M}{M_\odot} \quad (5.10)$$

Indicating that a sub-extremal magnetic black hole can consume a $\sim 2M_\odot$ neutron star within a time t

$$t = 0.8 \text{ Gyr} \left(\frac{M}{10^{22} \text{ g}} \right)^{-2} \quad (5.11)$$

A sub-extremal magnetic black hole with a mass above $\sim 10^{22}$ g can easily consume a neutron star within 1 Gyr, causing it to collapse into a black hole below the lower mass limit on a black hole formed from a collapsing star.

Only magnetic black holes that get caught in neutron stars will be able to consume them. Using (3.4), $E_f \sim 100$ MeV, $n_e \sim 10^{36} \text{ cm}^{-3}$, and an infalling velocity of $v \sim 0.3$ for a $r = 10 \text{ km}$ neutron star [61] we find that magnetic black holes that satisfy

$$q \geq 10^{-16} \left(\frac{M}{10^{22} \text{ g}} \right)^{-1/2} \quad (5.12)$$

will get caught inside of a neutron star they pass through.

Based on the black hole accumulation rate in neutron stars presented in (4.15) magnetic black holes that are heavy enough to collapse a neutron star ($M > 10^{22}$ g), and that satisfy (5.12), would not be abundant enough to observably alter the neutron star abundance, even if they constituted all of dark matter. Only $1.4 \times 10^{-5} f (10^{22} \text{ g}/M) \left(\frac{T}{\text{Gyr}} \right)$ of neutron stars, where T is the age of the neutron star, would have captured a charged black hole. Regardless, magnetically charged black holes do offer a new mechanism for producing black holes in the "mass gap" mass range.

6 Conclusion

In this work we have extensively explored the phenomenology of EMBHs and of stable magnetically charged black holes. We have placed stringent bounds on the abundance of these objects based on their ability to destroy white dwarfs either by initiating supernovae for EMBHs with masses below 4×10^{12} g, or by consuming them, for charged black holes with masses above 10^{17} g. We also derived the bounds which apply to both extremal and non-extremal magnetic black holes based on their overheating of warm ionized gas cloud in the Milky Way. We carefully detailed how EMBHs might merge, and the observable emission from these mergers. We provided minimal model independent constraints for EMBHs that catalyze nucleon decay, while leaving a precise calculation of the catalysis

cross section for future work. As in [12] and [13] we leave a detailed exploration of how EMBHs might form to future work as well.

One possibly interesting area we did not address is the connection between primordial EMBHs and primordial magnetic fields. It has been recently suggested the primordial magnetic fields present just before recombination could reduce the Hubble tension by altering the way charged particles cluster [84]. Additionally, many models of galactic magnetic field formation rely on the presence of a small seed field around the time of galaxy collapse [85]. The seed fields needed to generate the μG magnetic fields observed in galaxies today vary with the particular model, but reach as low as 10^{-30}G fields coherent over distances of $\gtrsim 100\text{ pc}$ [86]. EMBHs and charged black holes carry high magnetic charges and can generate reasonably strong magnetic fields coherent over the average separation between them.

Taking the typical EMBH separation, one can estimate typical magnetic fields due to EMBHs:

$$B \sim \frac{4}{3} \left(\frac{4\pi\rho_{DM}f\Delta}{3M} \right)^{2/3} Q(1+z)^2 \sim 1.5 * 10^{-23}\text{G} (f\Delta)^{2/3} q \left(\frac{M}{g} \right)^{1/3} (1+z) \quad (6.1)$$

where Δ is the local EMBH overdensity. Such a field would be coherent over length scales

$$l \sim \left(\frac{3M}{4\pi\rho_{DM}f\Delta} \right)^{1/3} \sim 1.5 * 10^{-9}\text{pc} \left(\frac{M}{g} \right)^{1/3} \frac{(f\Delta)^{-1/3}}{(1+z)} \quad (6.2)$$

Indicating that there are some unconstrained regions of parameter space where magnetic black holes could play a role in galactic magnetic field formation.

There is still much to understand about EMBHs. How exactly small EMBHs accumulate matter, whether nucleon catalysis happens and the exact details of such a process are not yet understood. While it is quite clear that EMBHs cannot constitute a meaningful fraction of the dark matter, they remain long lived, well-motivated, and very simple extensions of the standard model. They can offer new mechanisms for heating galactic plasma, producing gamma rays, initiating supernovae, and generating neutron star mass black holes. EMBHs remain interesting tools to consider for many current and future astrophysical questions.

Acknowledgements We would like to thank Emanuele Berti, Rob Farmer, Michael Fedderke, Ely Kovetz, Michael Shara, and Raman Sundrum for their insightful conversations and guidance. Special thanks to Leandro Althaus for sharing their detailed analysis of white dwarf interior compositions. This work was supported in part by the National Science Foundation under grant PHY-1818899.

A EMBH Friction with a Fermi Gas at Finite Temperatures

The friction between a magnetic charge and an electron fermi gas at finite temperature can be found by modifying the derivation presented in [29]. The energy of electrons that scatter off of a passing monopole will change by $\Delta E = pv(\cos(\theta) - \cos(\theta'))$ where θ is the angle

between the velocity of the incoming electron and the monopole velocity v , θ' is the angle between the scattered electron's velocity and v , p is the momentum of the electron. The energy given to an EMBH from all of the scattering electrons can be found by integrating:

$$\frac{dE}{dx} = \int_{E, \theta, \theta', \Psi, \phi} n(E) (1 - f(E + \Delta E)) \frac{d\sigma}{d\Omega} \Delta E \frac{\sin(\theta) \sin(\theta') \sin(\Psi) d\theta d\theta' d\Psi d\phi}{4\pi} \quad (\text{A.1})$$

Here

$$n(E) = \frac{m_e}{\pi^2} \sqrt{2m_e E} \times \frac{1}{\exp\left(\frac{E - E_f}{T}\right) + 1} \quad (\text{A.2})$$

is the number density of electrons with energy E in a fermi gas at temperature T and with a fermi energy E_f .

$$f(E) = \frac{1}{\exp\left(\frac{E - E_f}{T}\right) + 1} \quad (\text{A.3})$$

represents the fraction of energy states that are available at the energy the electrons would scatter into. Electrons can only scatter into available energy states, which is why this term is needed. The scattering cross section $\frac{d\sigma}{d\Omega}$ is analogous to a Rutherford scattering cross section [29]

$$\frac{d\sigma}{d\Omega} = \frac{Q^2 e^2}{4p^2 \sin^4(\Psi/2)} \quad (\text{A.4})$$

where $\cos(\Psi) = \sin(\theta) \sin(\theta') \cos(\Delta\phi) + \cos(\theta) \cos(\theta')$. Ψ is the angle between the velocities of the incoming and scattered electron. The integral over Ψ diverges as a log as Ψ approaches zero. We cut off the integral over Ψ at $\Psi_{\min} = \frac{\nu_{\sigma}^{ie}}{2E_f}$ which limits the scattering angle by the scattering length in the medium as suggested in [29]. Using this cutoff allows one to integrate (A.1) over Ψ and ϕ , giving $16\pi \log(\frac{1}{\Psi})$. Substituting $x = \cos(\theta)$ and $y = \cos(\theta')$ gives:

$$\frac{dE}{dx} = \frac{Ge^2 \sqrt{2m_e} M^2}{\pi^2} \text{Log} \left[\frac{2E_f}{\nu_{\sigma}^{ei}} \right] \times \int_{-1}^1 \int_{-1}^1 \int_0^\infty \sqrt{E} \times f(E) (1 - f(E + \Delta E)) dx dy dE \quad (\text{A.5})$$

B Calculation Details for Binary Mergers

B.1 Derivation of the Merger Time for a Magnetically Charged Binary

The merger rate for an EMBH binary can be found by considering the electromagnetic radiation emitted as the EMBHs orbit each other. EMBHs moving through an orbit radiate as two perpendicular oscillating magnetic dipoles. Energy losses via gravitational radiation come from the binary system's quadrupole moment, and are therefore subdominant to electromagnetic energy losses. The binary emission rate for black holes of arbitrary electric charge and mass in circular orbits is presented in [87]. The merger rate for charged black holes in a circular orbit is also considered in [13].

The electric and magnetic fields of two perpendicular magnetic dipoles oriented in the x and z plane which vary arbitrarily with time is:

$$\begin{aligned}
B = & \frac{2\cos(\theta)}{r^2} \left[\frac{1}{r} + \frac{d}{d\tau} \right] (p_x(\tau) + p_z(\tau)) \hat{r} \\
& + \frac{1}{r} \left[\frac{1}{r^2} + \frac{1}{r} \frac{d}{d\tau} + \frac{d^2}{d\tau^2} \right] \left(-\sin(\theta)p_z(\tau) + \cos(\theta)\cos(\phi)p_x(\tau) \right) \hat{\theta} \\
& - \frac{\sin(\phi)}{r} \left[\frac{1}{r^2} + \frac{1}{r} \frac{d}{d\tau} + \frac{d^2}{d\tau^2} \right] p_x(\tau) \hat{\phi}
\end{aligned} \tag{B.1}$$

$$\begin{aligned}
E = & -\frac{\sin(\phi)}{r} \left[\frac{1}{r} \frac{d}{d\tau} + \frac{d^2}{d\tau^2} \right] p_x(\tau) \\
& + \frac{1}{r} \left[\frac{1}{r} \frac{d}{d\tau} + \frac{d^2}{d\tau^2} \right] \left(\sin(\theta)p_z(\tau) + \cos(\theta)\cos(\phi)p_x(\tau) \right) \hat{\phi}
\end{aligned}$$

Where $p_z(\tau)$ and $p_x(\tau)$ are the dipole moments as a function of the retarded time $\tau = t - r$ where r is the radius from the center of the dipole. The angular coordinates are defined from the z axis. The energy loss is found by taking $P = \int \frac{1}{4\pi} (E \times B) \cdot dA$ at $r = \infty$. Changes to the shape of the orbit are described by changes to the angular momentum along the y axis, which can be described by $\frac{dL_y}{dt} = \frac{1}{4\pi} \int \hat{y} \cdot (r \times (E \times B)) dA$ integrated over a sphere at $r = \infty$. Using the terms from equation B.1, this gives:

$$P = \frac{2}{3} \left[\left(\frac{d^2}{d\tau^2} p_x(\tau) \right)^2 + \left(\frac{d^2}{d\tau^2} p_z(\tau) \right)^2 \right] \tag{B.2}$$

$$\frac{L_y}{dt} = \frac{2}{3} \left[\frac{d^2 p_x}{d\tau^2} \frac{dp_z}{d\tau} + \frac{d^2 p_z}{d\tau^2} \frac{dp_x}{d\tau} \right]$$

To use these expressions to get a merger time, one must parameterize the dipole moments in terms of orbital parameters of the binary system. Each monopole moves about the center of mass of the system with an angular velocity:

$$\dot{\psi} = \sqrt{\frac{2G(m_1 + m_2)}{a^3(1 - e^2)^3}} (1 + e\cos\psi)^2 \tag{B.3}$$

where ψ is the angular location of the monopole along its orbital trajectory as defined by the positive z axis, a is the semimajor axis of the orbit, e is the eccentricity, and m_1 and m_2 are the masses of each EMBH. EMBHs feel an equal mutual magnetic and gravitational attractive force, which is accounted for by the extra factor of 2 in the above expression. The distance of an EMBH from the center of mass of the system, d , is set by:

$$d = \frac{a(1 - e^2)}{1 + e\cos\psi} \tag{B.4}$$

In terms of these parameters the dipole moments are:

$$\begin{aligned}
p_z(\tau) &= 2Qd(\tau)\cos\psi \\
p_x(\tau) &= 2Qd(\tau)\sin\psi
\end{aligned} \tag{B.5}$$

Using these expressions, all of the time derivatives of the dipole moments can be found in terms a , e , and ψ . Putting these into equation B.2 gives:

$$P = \frac{32G^2Q^2(m_1 + m_2)^2}{3a^4(1 - e^2)^4}(1 + e\cos\psi)^4 \quad (\text{B.6})$$

$$\frac{dL_y}{dt} = \frac{8Q^2(2G(m_1 + m_2))^{3/2}}{3a^{5/2}(1 - e^2)^{5/2}}(1 + e\cos\psi)^3$$

Averaging the energy and angular momentum losses over a single orbit gives

$$\langle P \rangle = -\frac{4Q^2G^2(m_1 + m_2)^2}{a^4(1 - e^2)^4}\left(\frac{8}{3} + 8e^2 + e^4\right) \quad (\text{B.7})$$

$$\left\langle \frac{dL_y}{dt} \right\rangle = -\frac{Q^2(2G(m_1 + m_2))^{3/2}}{a^{5/2}(1 - e^2)^{5/2}}\left(\frac{8}{3} + 4e^2\right)$$

For comparison to the energy losses from gravitational radiation, we rewrite these assuming $m_1 = m_2 = M$ and that $Q = \frac{M}{m_P}$ where m_P is the plank mass and $m_P^{-2} = G$

$$\langle P \rangle = -\frac{16M^4G^3}{a^4(1 - e^2)^4}\left(\frac{8}{3} + 8e^2 + e^4\right) \quad (\text{B.8})$$

$$\left\langle \frac{dL_y}{dt} \right\rangle = -\frac{M^{7/2}2^{3/2}G^{5/2}}{a^{5/2}(1 - e^2)^{5/2}}\left(\frac{8}{3} + 4e^2\right)$$

In comparison the power output from gravitational waves for an EMBH binary is $\langle P \rangle = \frac{1024}{5} \frac{G^4 M^5}{a^5(1 - e^2)^{7/2}} \left(1 + \frac{73}{24}e^2 + \frac{37}{96}e^4\right)$ [88]. The extra factor of 16 comes from enhancements to the energy and angular momentum of the binary due to the increase in attraction between the EMBHs as compared to uncharged black holes. This is very subdominant to the power lost to EM radiation. Gravitational radiation will only match EM radiation once a drops down to $\frac{12}{5}r_s$ where r_s is the Schwarzschild radius. We conclude that gravitational radiation does little to alter the lifetime of EMBH binaries. EM radiation remains significant down to the Schwarzschild radius, with the power radiated by EM radiation being only a factor of $\frac{32}{5} = 6.4$ smaller than the power emitted by gravitational radiation.

The energy of the system is related to the semimajor axis by $E = \frac{Gm^2}{a}$. This is twice the energy of a neutral black hole system of the same mass. The extra factor of two coming from the extra attractive force between the EMBH. The average rate of energy loss can be related to the average change in the semimajor axis by $\langle P \rangle = \frac{GM^2}{a^2} \left\langle \frac{da}{dt} \right\rangle$, which gives;

$$\left\langle \frac{da}{dt} \right\rangle = \frac{16G^2M^2}{a^2(1 - e^2)^4} \left(\frac{8}{3} + 8e^2 + e^4\right) \quad (\text{B.9})$$

For $e = 0$ one can solve for the merger time analytically, noting that the separation between the two black holes will be twice the semimajor axis of either black hole's orbit.

$$t_{m0} = \frac{a_0^3}{128G^2M^2} = 4.8 \times 10^{49} s \frac{(a_0/\text{m})^3}{(M/\text{g})^2} \quad (\text{B.10})$$

where a_0 is the initial semi-major axis.

For comparison, the merger time if only the gravitational radiation were considered would be

$$t_{Gm0} = \frac{5}{512\sqrt{2}} \frac{a^4}{G^3 M^3} = 5.8 \times 10^{79} s \frac{(a_0/m)^4}{(M/g)^3} \quad (\text{B.11})$$

For cases in which $e \neq 0$ one must also determine the evolution of the eccentricity in order to determine the spin down time. Using $L^2 = M^3 a(1 - e^2)$ gives the relation

$$L \left\langle \frac{dL}{dt} \right\rangle = GM^3 \left((1 - e^2) \left\langle \frac{da}{dt} \right\rangle - 2ae \left\langle \frac{de}{dt} \right\rangle \right) \quad (\text{B.12})$$

which can be rearranged to solve for $\langle \frac{de}{dt} \rangle$

$$\left\langle \frac{de}{dt} \right\rangle = \frac{8G^2 M^2}{a^3 (1 - e^2)^3} \left(\frac{20}{3} e + 5e^3 \right) \quad (\text{B.13})$$

Equations (B.9) and (B.13) can be used to find

$$\left\langle \frac{da}{de} \right\rangle = \frac{2a}{(1 - e^2)} \frac{\left(\frac{8}{3} + 8e^2 + e^4 \right)}{\left(\frac{20}{3} e + 5e^3 \right)} \quad (\text{B.14})$$

Integrating equation B.14 gives a as a function of e :

$$a = a_0 \frac{(1 - e_0^2)}{e_0^{4/5} (3e_0^2 + 4)^{2/5}} \frac{e^{4/5} (3e^2 + 4)^{2/5}}{(1 - e^2)} \quad (\text{B.15})$$

Where a_0 and e_0 are the starting semimajor axes and eccentricities of the system. Finally, equation B.15 can be plugged into equation B.13 and integrated to get a general expression of the merger time as a function of the initial semimajor axis and eccentricity of a binary system

$$t_m = \frac{a_0^3}{8G^2 M^2} \frac{(1 - e_0^2)^3}{e_0^{12/5} (3e_0^2 + 4)^{6/5}} \int_0^{e_0} e^{7/5} \frac{(3e'^2 + 4)^{6/5}}{\left(\frac{20}{3} + 5e'^2 \right)} de' \quad (\text{B.16})$$

In the limit that $e_0 \sim 1$ the integral over e becomes ~ 0.035 . Taking the overall limit $e_0 \sim 1$ gives

$$t_m = \frac{0.034 a_0^3}{8G^2 M^2} (1 - e_0^2)^3 \quad (\text{B.17})$$

B.2 Derivation of the EMBH Binary Merger Rate

This derivation of the EMBH merger rate follows similar derivations for the merger rate of uncharged black hole binaries [89, 90], though modified to account for effects from the extremal magnetic fields of the black holes. The initial orbital parameters of binaries, their semi-major axes a_0 , and eccentricities e_0 are characterized by their comoving separation x , the comoving distance to the next nearest EMBH y and the redshift z_d when the binary decouples from the Hubble flow.

When friction with the thermal bath is not important, we assume the EMBH binaries decouple from the Hubble flow, and form a stable binary when the time needed for the

EMBHs to free fall into each other becomes less than the Hubble time [89, 90]. During radiation domination this corresponds to a decoupling redshift z_d of

$$(1 + z_d) = \frac{3M(1 + z_{eq})}{4\pi\rho_{dm}x^3} = \frac{k_d}{x^3} \quad (\text{B.18})$$

Where we denote $k_d \equiv \frac{3(1+z_{eq})}{4\pi\rho_{dm}}$. EMBH lose energy as they pass through a plasma by exciting eddy currents. This creates a friction between the EMBH and the plasma. The infall dynamics change when friction with the thermal bath becomes greater than the Hubble acceleration. In this scenario we consider the binary decoupled when the EMBH terminal infall velocity exceeds the Hubble velocity $v_H = \frac{H(z)x}{(1+z)}$. The terminal infall velocity is found by balancing the attractive force between the EMBHs, $\frac{2GM^2(1+z)^2}{x^2}$, with the frictional force exerted by the plasma on the black holes.

The frictional force between a magnetic monopole and a plasma is described in [21] We adapt it here for an EMBH with mass M

$$\left(\frac{dE}{dx}\right)_f = -\frac{16\pi^{1/2}e^2n_e(z)}{3\sqrt{2T(z)m_e}}GM^2V\left[\log(4\pi n_e(z)L_D^2l) + \frac{2}{3}\right] \quad (\text{B.19})$$

Where n_e is the electron number density, which we take to be $\sim (1+z)^3 \frac{\rho_{c0}\Omega_b}{m_{pr}}$ in the thermal bath where ρ_{c0} is the critical density today, Ω_b is the baryon fraction and m_{pr} is the proton mass, T is the gas temperature which we take to be $\sim 2.7(1+z)\text{K}$, V is the velocity of the monopole, $L_D = \sqrt{\frac{T}{4\pi n_e e^2}}$ is the plasma Debye length, and $l = \left(\frac{2T}{\pi m_e}\right)^{1/4} \frac{1}{V^{1/2}\omega_p}$ is the attenuation length of the plasma and ω_p is the plasma frequency. To simplify comparing forces we will represent $(\frac{dE}{dx})_f$ as $m^2V(1+z)^{5/2}\mathcal{F}$. \mathcal{F} represents the *mostly* z , m and V independent component of $(\frac{dE}{dx})_f$

If $\mathcal{F}z^{5/2}M > H(z)$ at the regular decoupling redshift z_d , then the EMBHs will continue moving apart with the Hubble flow until $\frac{2G}{x^2(1+z)^{1/2}\mathcal{F}} = \frac{H(z)x}{(1+z)}$. During radiation domination this gives a decoupling redshift z_b of

$$(1 + z_b) = \left(\frac{2G}{H_0\sqrt{\Omega_r}\mathcal{F}}\right)^{2/3} x^{-2} = k_b x^{-2} \quad (\text{B.20})$$

Where we will denote $k_b \equiv \left(\frac{H_0\sqrt{\Omega_r}\mathcal{F}}{2G}\right)^{2/3}$, and where Ω_r is the fraction of the critical energy density composed of radiation at $z = 0$ and z_f denotes the redshift at which frictional forces become small compared to Hubble:

$$(1 + z_f) = \frac{\mathcal{F}M^2}{H_0\sqrt{\Omega_r}} \quad (\text{B.21})$$

Binaries must decouple by matter radiation equality because the ratio between the free fall time and the Hubble time becomes constant during matter domination, so those binaries that could not decouple by matter radiation equality will not gain the ability to do so during matter domination,

The semimajor axis of the binary a_0 is just $\frac{x}{(1+z_d)}$. The eccentricity e_0 of the binary is set by interactions with nearest EMBH outside of the binary. One of the EMBHs in the

binary gets pulled out of its free fall path by the next nearest EMBH, while the other does not strongly feel any forces from the next nearest charge. The distance the in-falling EMBH gets pulled out of its free fall path will set the semi-minor axis for the binary system b . This can be calculated by multiplying the force exerted by the EMBH nearest the binary with the square of the time it takes the perturbed EMBH to fall a distance a_0 . Setting the comoving distance to the nearest EMBH outside of the binary to y this approach gives a b of

$$2b = \frac{1}{2} \left(\frac{2Gm(1+z_d)^2}{y^2} \right) \left(\frac{x^3}{4GM(1+z_d)^3} \right) = \frac{x^2}{y^2} a \quad (\text{B.22})$$

This gives a starting eccentricity of

$$e_0 = \sqrt{1 - \frac{x^4}{4y^4}} \quad (\text{B.23})$$

The probability that two oppositely charged EMBHs are separated by a co-moving distance between x and $x + dx$ and that the next nearest EMBH of any sign charge is between y and $y + dy$.

$$dP = \frac{1}{2} (4\pi n)^2 x^2 y^2 dx dy \quad (\text{B.24})$$

where n is the comoving number density of EMBH. The factor of $\frac{1}{2}$ arises because each EMBH can only pair with an oppositely charged partner, so the average distance between "pairable" EMBHs is $2^{1/3}$ times the average distance between all EMBH. x is by definition less than y , because a binary would just form with the EMBHs separated by y otherwise. y can be at most the average separation between EMBH. This defines y_{max}

$$y_{max} = \frac{3M}{4\pi\rho_{dm}f} \quad (\text{B.25})$$

This can be re-written using (B.18) and (B.23) to give a probability distribution for the orbital parameters of all of the binaries. That can then be related to the probability that a binary merges at a specific time t_m by (B.17) which is derived in Section B.1. Rearranging (B.17) gives $a_0(t_m, e_0)$, the starting semi-major axis that corresponds to a binary with eccentricity e_0 that would merge in t_m .

$$a_0 = \frac{M^{2/3} t_m^{1/3}}{\left(\frac{0.034}{8G^2}\right)^{1/3} (1 - e_0^2)} \quad (\text{B.26})$$

All binaries that merge at t_m have parameters that lie along the curve in $e - a$ space $a_0(t_m, e_0)$. With a bit of algebra, one finds that in the limit where $e \sim 1$ the probability that an EMBH binary merges between t_m and $t_m + dt$ is

$$dP = \frac{(4\pi n_{bh})^2}{3 * 2^{13/2}} \frac{1}{k_d^{3/2} \left(\frac{0.034}{8G^2}\right)^{1/2}} \frac{M}{t_m^{1/2}} \frac{e_0}{(1 - e_0^2)^{13/4}} dt de \quad (\text{B.27})$$

The merger rate per EMBH, Γ_m at a specific time t_m can be found then by integrating $\frac{dP}{dt}$ over all eccentricities a binary merging at t_m could have.

$$\Gamma_m = \frac{dP}{dt} = \frac{(4\pi\rho_{DM}f)^2}{27 * 2^{11/2}} \frac{1}{k_d^{3/2} \left(\frac{0.034}{8G^2}\right)^{1/2}} \frac{1}{Mt_m^{1/2}} \left(\frac{1}{(1 - e_{max}^2)^{9/4}} - \frac{1}{(1 - e_{min}^2)^{9/4}} \right) \quad (\text{B.28})$$

Multiplying Γ_m by n_{bh} , the proper number density of EMBHs at t_m , would give the rate at which EMBH mergers happen at t_m . The bounds used in these integrals e_{max} and e_{min} are the largest and smallest eccentricities a binary merging at t_m could have.

We find the limits on eccentricities as follows. We define e_{upper} as the highest eccentricity a binary with semi-major axis a can have. This limit exists because y cannot be greater than the average spacing between EMBHs $y_{max} = \left(\frac{3m}{4\pi\rho_{dm}f}\right)^{1/3}$. This gives

$$e_{upper} = \sqrt{1 - \frac{a}{4k_d y_{max}^4}} \quad (\text{B.29})$$

Then, e_{max} is set by where the curve $a(e_0, t_m)$, intersects e_{upper} , or a_{eq} , the semi-major axis of a binary that decouples at the latest allowed decoupling redshift z_{eq} .

$$e_{max} = \begin{cases} \sqrt{1 - \left(\frac{M^{2/3} t_m^{1/3}}{4k_d \left(\frac{0.034}{8G^2}\right)^{1/3} y_m^4}\right)^{1/2}} & t_m \leq T_c \\ \sqrt{1 - \left(\frac{k_d M^2 t_m (1+z_{eq})^4}{\left(\frac{0.034}{8G^2}\right)}\right)^{1/3}} & t_m > T_c \end{cases} \quad (\text{B.30})$$

where T_c is

$$T_c = \frac{\frac{0.034}{8G^2}}{2^6 M^2 k_d^5 y_m^{12} (1+z_{eq})^8} \quad (\text{B.31})$$

Finally, e_{min} is the lowest eccentricity a binary that merges in t_m and decouples after z_f can have. It is 0 when all binaries that merge in t_m decouple after z_f .

$$e_{min} = \begin{cases} \sqrt{1 - \left(\frac{k_d M^2 t_m (1+z_f)^4}{\left(\frac{0.034}{8G^2}\right)}\right)^{1/3}} & t_m > T_f \\ 0 & t_m < T_f \end{cases} \quad (\text{B.32})$$

where T_f is

$$T_f = \frac{\left(\frac{0.034}{8G^2}\right)}{M^2 k_d (1+z_f)^4} \quad (\text{B.33})$$

Here e_{min} is determined in the limit that $e_{min} \sim 1$, this is appropriate because the majority of binaries merging today or earlier are highly eccentric.

Bibliography

- [1] G. 't Hooft, *Magnetic monopoles in unified gauge theories*, *Nuclear Physics B* **79** (1974) 276.
- [2] A.M. Polyakov, *Particle Spectrum in the Quantum Field Theory*, *JETP Lett.* **20** (1974) 194.
- [3] MACRO collaboration, *Final results of magnetic monopole searches with the MACRO experiment*, *Eur. Phys. J. C* **25** (2002) 511 [[hep-ex/0207020](#)].
- [4] S. Orito, H. Ichinose, S. Nakamura, K. Kuwahara, T. Doke, K. Ogura et al., *Search for supermassive relics with a 2000-m² array of plastic track detectors*, *Phys. Rev. Lett.* **66** (1991) 1951.

- [5] S. Balestra, S. Cecchini, M. Cozzi, M. Errico, F. Fabbri, G. Giacomelli et al., *Magnetic monopole search at high altitude with the slim experiment*, [*The European Physical Journal C* **55** \(2008\) 57–63](#).
- [6] A.H. Guth, *Inflationary universe: A possible solution to the horizon and flatness problems*, [*Phys. Rev. D* **23** \(1981\) 347](#).
- [7] J. Preskill, *Cosmological Production of Superheavy Magnetic Monopoles*, [*Phys. Rev. Lett.* **43** \(1979\) 1365](#).
- [8] B.J. Carr and S. Hawking, *Black holes in the early Universe*, *Mon. Not. Roy. Astron. Soc.* **168** (1974) 399.
- [9] A.H. Guth and S.H.H. Tye, *Phase transitions and magnetic monopole production in the very early universe*, [*Phys. Rev. Lett.* **44** \(1980\) 631](#).
- [10] J. Callan, Curtis G. and E. Witten, *Monopole Catalysis of Skyrminion Decay*, [*Nucl. Phys. B* **239** \(1984\) 161](#).
- [11] V. Rubakov, *Adler-Bell-Jackiw Anomaly and Fermion Number Breaking in the Presence of a Magnetic Monopole*, [*Nucl. Phys. B* **203** \(1982\) 311](#).
- [12] Y. Bai, J. Berger, M. Korwar and N. Orlofsky, *Phenomenology of magnetic black holes with electroweak-symmetric coronas*, 2020.
- [13] D. Ghosh, A. Thalappilil and F. Ullah, *Astrophysical hints for magnetic black holes*, 2020.
- [14] J. Maldacena, *Comments on magnetic black holes*, [2004.06084](#).
- [15] P.A.M. Dirac, *Quantised Singularities in the Electromagnetic Field*, [*Proceedings of the Royal Society of London Series A* **133** \(1931\) 60](#).
- [16] S.W. Hawking, *Black hole explosions?*, [*Nature* **248** \(1974\) 30](#).
- [17] D.L.J. Ho and A. Rajantie, *The electroweak sphaleron in a strong magnetic field*, 2020.
- [18] E. Poisson and W. Israel, *Inner-horizon instability and mass inflation in black holes*, [*Phys. Rev. Lett.* **63** \(1989\) 1663](#).
- [19] D.E. Kaplan and S. Rajendran, *Firewalls in general relativity*, [*Physical Review D* **99** \(2019\) .](#)
- [20] N. Lehner, B. Wakker and B. Savage, *CII radiative cooling of the diffuse gas in the Milky Way*, [*Astrophys. J.* **615** \(2004\) 767 \[astro-ph/0407363\]](#).
- [21] N. Meyer-Vernet, *Energy loss by slow magnetic monopoles in a thermal plasma*, [*The Astrophysical Journal* **290** \(1985\) 21](#).
- [22] C.F. McKee and J.P. Ostriker, *A theory of the interstellar medium: three components regulated by supernova explosions in an inhomogeneous substrate.*, [*The Astrophysical Journal* **218** \(1977\) 148](#).
- [23] F.X. Timmes and S.E. Woosley, *The Conductive Propagation of Nuclear Flames. I. Degenerate C + O and O + NE + MG White Dwarfs*, [*The Astrophysical Journal* **396** \(1992\) 649](#).
- [24] R. Janish, V. Narayan and P. Riggins, *Type Ia supernovae from dark matter core collapse*, [*Phys. Rev. D* **100** \(2019\) 035008 \[1905.00395\]](#).
- [25] M.A. Fedderke, P.W. Graham and S. Rajendran, *White dwarf bounds on charged massive particles*, [*Physical Review D* **101** \(2020\) .](#)

- [26] M.A. Hollands, P.-E. Tremblay, B.T. Gänsicke, M.E. Camisassa, D. Koester, A. Aungwerojwit et al., *An ultra-massive white dwarf with a mixed hydrogen–carbon atmosphere as a likely merger remnant*, *Nature Astronomy* **4** (2020) 663–669.
- [27] P. Dufour, S. Blouin, S. Coutu, M. Fortin-Archambault, C. Thibeault, P. Bergeron et al., *The Montreal White Dwarf Database: A Tool for the Community*, in *20th European White Dwarf Workshop*, P.E. Tremblay, B. Gänsicke and T. Marsh, eds., vol. 509 of *Astronomical Society of the Pacific Conference Series*, p. 3, Mar., 2017 [[1610.00986](#)].
- [28] L. Siess, *Evolution of massive AGB stars. II. model properties at non-solar metallicity and the fate of Super-AGB stars*, *Astronomy and Astrophysics* **476** (2007) 893.
- [29] S.P. Ahlen and K. Kinoshita, *Calculation of the stopping power of very-low-velocity magnetic monopoles*, *Phys. Rev. D* **26** (1982) 2347.
- [30] A.Y. Potekhin, D.A. Baiko, P. Haensel and D.G. Yakovlev, *Transport properties of degenerate electrons in neutron star envelopes and white dwarf cores*, *Astron. Astrophys.* **346** (1999) 345 [[astro-ph/9903127](#)].
- [31] F. D’Antona and I. Mazzitelli, *Cooling of white dwarfs*, *Ann. Rev. Astron. Astrophys.* **28** (1990) 139.
- [32] S. Bagnulo and J.D. Landstreet, *Searching for the weakest detectable magnetic fields in white dwarfs. Highly-sensitive measurements from first VLT and WHT surveys*, *Astronomy and Astrophysics* **618** (2018) A113 [[1807.09649](#)].
- [33] A. Kawka, *The properties and origin of magnetic fields in white dwarfs*, *Contributions of the Astronomical Observatory Skalnaté Pleso* **48** (2018) 228 [[1801.05602](#)].
- [34] J. Braithwaite and H.C. Spruit, *A fossil origin for the magnetic field in a stars and white dwarfs*, *Nature* **431** (2004) 819–821.
- [35] J. Nordhaus, S. Wellons, D.S. Spiegel, B.D. Metzger and E.G. Blackman, *Formation of high-field magnetic white dwarfs from common envelopes*, *Proceedings of the National Academy of Sciences* **108** (2011) 3135–3140.
- [36] FERMI-LAT collaboration, *The spectrum of isotropic diffuse gamma-ray emission between 100 MeV and 820 GeV*, *Astrophys. J.* **799** (2015) 86 [[1410.3696](#)].
- [37] T. Ukwatta, D. Stump, J. Linnemann, J. MacGibbon, S. Marinelli, T. Yapici et al., *Primordial black holes: Observational characteristics of the final evaporation*, *Astroparticle Physics* **80** (2016) 90–114.
- [38] K.V. Berghaus, M.D. Diamond and D. Kaplan, *Decays of Long-Lived Relics and Their Signatures at IceCube*, *JHEP* **05** (2019) 145 [[1811.04939](#)].
- [39] A.A. Zdziarski and R. Svensson, *Absorption of X-Rays and Gamma Rays at Cosmological Distances*, *The Astrophysical Journal* **344** (1989) 551.
- [40] M. Lewis, K. Freese and G. Tarle, *Protogalactic extension of the Parker bound*, *Phys. Rev. D* **62** (2000) 025002 [[astro-ph/9911095](#)].
- [41] F.C. Adams, M. Fatuzzo, K. Freese, G. Tarlé, R. Watkins and M.S. Turner, *Extension of the parker bound on the flux of magnetic monopoles*, *Phys. Rev. Lett.* **70** (1993) 2511.
- [42] M.S. Turner, E.N. Parker and T. Bogdan, *Magnetic Monopoles and the Survival of Galactic Magnetic Fields*, *Phys. Rev. D* **26** (1982) 1296.

- [43] A. Bonafede, F. Vazza, M. Brüggén, M. Murgia, F. Govoni, L. Feretti et al., *Measurements and simulation of Faraday rotation across the Coma radio relic*, *Mon. Not. Roy. Astron. Soc.* **433** (2013) 3208 [[1305.7228](#)].
- [44] M. Kierdorf, R. Beck, M. Hoeft, U. Klein, R.J. van Weeren, W.R. Forman et al., *Relics in galaxy clusters at high radio frequencies*, *Astronomy and Astrophysics* **600** (2017) A18.
- [45] J. Derkaoui, G. Giacomelli, T. Lari, G. Mandrioli, M. Ouchrif, L. Patrizii et al., *Energy losses of magnetic monopoles and dyons in scintillators, streamer tubes and nuclear track detectors*, *Astropart. Phys.* **10** (1999) 339.
- [46] J. Arafune and M. Fukugita, *Velocity-dependent factors for the rubakov process for slowly moving magnetic monopoles in matter*, *Phys. Rev. Lett.* **50** (1983) 1901.
- [47] L. Bracci and G. Fiorentini, *Interactions of Magnetic Monopoles With Nuclei and Atoms: Formation of Bound States and Phenomenological Consequences*, *Nucl. Phys. B* **232** (1984) 236.
- [48] K. Olaussen, H.A. Olsen, I. Overbo and P. Osland, *PROTON CAPTURE BY MAGNETIC MONOPOLES*, *Phys. Rev. Lett.* **52** (1984) 325.
- [49] L.G. Althaus, A.H. Córscico and F. De Gerónimo, *Effect of Coulomb diffusion of ions on the pulsational properties of DA white dwarfs*, *Astronomy and Astrophysics* **644** (2020) A55 [[2010.11131](#)].
- [50] K. Freese, *DO MONOPOLES KEEP WHITE DWARFS HOT?*, *Astrophys. J.* **286** (1984) 216.
- [51] K.S. Thorne and R.D. Blandford, *Modern Classical Physics: Optics, Fluids, Plasmas, Elasticity, Relativity, and Statistical Physics* (2017).
- [52] S.E. Woosley, S. Wunsch and M. Kuhlen, *Carbon ignition in type ia supernovae: An analytic model*, *The Astrophysical Journal* **607** (2004) 921–930.
- [53] D.L. Turcotte and G. Schubert, *Geodynamics - 2nd Edition* (2002), [10.2277/0521661862](#).
- [54] F. D’Antona and I. Mazzitelli, *Cooling of white dwarfs.*, *Annual Review of Astron and Astrophys* **28** (1990) 139.
- [55] N.C. Hambly, S.J. Smartt and S.T. Hodgkin, *WD 0346+246: A Very Low Luminosity, Cool Degenerate in Taurus*, *The Astrophysical Journal* **489** (1997) L157.
- [56] J. Liebert, C.C. Dahn and D.G. Monet, *The Luminosity Function of White Dwarfs*, *The Astrophysical Journal* **332** (1988) 891.
- [57] M. Kilic, *Cool white dwarfs*, in *White Dwarf Atmospheres and Circumstellar Environments*, pp. 25–52, John Wiley & Sons, Ltd (2011), DOI [<https://onlinelibrary.wiley.com/doi/pdf/10.1002/9783527636570.ch2>].
- [58] M. Kilic, J.R. Thorstensen, P.M. Kowalski and J. Andrews, *11-12 gyr old white dwarfs 30 pc away*, *Monthly Notices of the Royal Astronomical Society: Letters* **423** (2012) L132–L136.
- [59] E.W. Kolb and M.S. Turner, *Limits from the Soft x-Ray Background on the Temperature of Old Neutron Stars and on the Flux of Superheavy Magnetic Monopoles*, *Astrophys. J.* **286** (1984) 702.
- [60] M. Kutschera, *Neutron stars: formation and structure.*, *Acta Physica Polonica B* **29** (1998) 25 [[astro-ph/9801235](#)].
- [61] J.A. Harvey, *Magnetic monopoles in neutron stars*, *Nuclear Physics B* **236** (1984) 255.

- [62] D. McCammon, D.N. Burrows, W.T. Sanders and W.L. Kraushaar, *The soft X-ray diffuse background.*, *The Astrophysical Journal* **269** (1983) 107.
- [63] B. Haskell and A. Sedrakian, *Superfluidity and Superconductivity in Neutron Stars*, vol. 457, pp. 401–454 (2018), DOI [[1709.10340](https://doi.org/10.10340)].
- [64] J.A. Harvey, M.A. Ruderman and J. Shaham, *Effects of neutron-star superconductivity on magnetic monopoles and core field decay*, *Phys. Rev. D* **33** (1986) 2084.
- [65] D.M. Sedrakian, A.D. Sedrakian and G.F. Zharkov, *Type i superconductivity of protons in neutron stars*, *Monthly Notices of the Royal Astronomical Society* **290** (1997) 203–207.
- [66] B. Haskell and A. Sedrakian, *Superfluidity and superconductivity in neutron stars*, *Astrophysics and Space Science Library* (2018) 401–454.
- [67] P. Landry, R. Essick and K. Chatziioannou, *Nonparametric constraints on neutron star matter with existing and upcoming gravitational wave and pulsar observations*, *Physical Review D* **101** (2020) .
- [68] E. Berti. Private Communication, 2020.
- [69] H.O. Silva, H. Sotani and E. Berti, *Low-mass neutron stars: universal relations, the nuclear symmetry energy and gravitational radiation*, *Monthly Notices of the Royal Astronomical Society* **459** (2016) 4378–4388.
- [70] F. Özel and P. Freire, *Masses, radii, and the equation of state of neutron stars*, *Annual Review of Astronomy and Astrophysics* **54** (2016) 401 [<https://doi.org/10.1146/annurev-astro-081915-023322>].
- [71] SUPER-KAMIOKANDE collaboration, *Search for GUT monopoles at Super-Kamiokande*, *Nucl. Phys. B Proc. Suppl.* **229-232** (2012) 540.
- [72] K. Abe, Y. Hayato, T. Iida, M. Ikeda, C. Ishihara, K. Iyogi et al., *Solar neutrino results in super-kamiokande-iii*, *Physical Review D* **83** (2011) .
- [73] G.W. Simon and R.B. Leighton, *Velocity Fields in the Solar Atmosphere. III. Large-Scale Motions, the Chromospheric Network, and Magnetic Fields.*, *The Astrophysical Journal* **140** (1964) 1120.
- [74] Z. Abraham and J. Iben, Icko, *More Solar Models and Neutrino Fluxes*, *The Astrophysical Journal* **170** (1971) 157.
- [75] R. Arlt, A. Sule and G. Rüdiger, *Stability of toroidal magnetic fields in the solar tachocline*, *Astronomy and Astrophysics* **461** (2007) 295.
- [76] MACRO collaboration, *Search for nucleon decays induced by GUT magnetic monopoles with the MACRO experiment*, *Eur. Phys. J. C* **26** 163 [[hep-ex/0207024](https://arxiv.org/abs/hep-ex/0207024)].
- [77] B.T. Draine, *Physics of the Interstellar and Intergalactic Medium* (2011).
- [78] F. "Timmes, "coldwd.tbz."
- [79] S. Grunau and V. Kagramanova, *Geodesics of electrically and magnetically charged test particles in the reissner-nordström space-time: Analytical solutions*, *Physical Review D* **83** (2011) .
- [80] B. Carr, K. Kohri, Y. Sendouda and J. Yokoyama, *Constraints on primordial black holes*, 2020.

- [81] LIGO SCIENTIFIC, VIRGO collaboration, *GW190814: Gravitational Waves from the Coalescence of a 23 Solar Mass Black Hole with a 2.6 Solar Mass Compact Object*, *Astrophys. J. Lett.* **896** (2020) L44 [[2006.12611](#)].
- [82] B. Dasgupta, R. Laha and A. Ray, *Low mass black holes from dark core collapse*, 2020.
- [83] C.B. Richards, T.W. Baumgarte and S.L. Shapiro, *Relativistic bondi accretion for stiff equations of state*, 2021.
- [84] K. Jedamzik and L. Pogosian, *Relieving the hubble tension with primordial magnetic fields*, 2020.
- [85] R. Beck and R. Wielebinski, *Magnetic Fields in the Milky Way and in Galaxies*, pp. 641–723 (2013), DOI [[1302.5663](#)].
- [86] A.-C. Davis, M. Lilley and O. Törnkvist, *Relaxing the bounds on primordial magnetic seed fields*, *Phys. Rev. D* **60** (1999) 021301.
- [87] L. Liu, O. Christiansen, Z.-K. Guo, R.-G. Cai and S.P. Kim, *Gravitational and Electromagnetic Radiations from Binary Black Holes with Electric and Magnetic Charges: I. Circular Orbits on a Poincaré Cone*, [2008.02326](#).
- [88] P.C. Peters and J. Mathews, *Gravitational radiation from point masses in a keplerian orbit*, *Phys. Rev.* **131** (1963) 435.
- [89] M. Sasaki, T. Suyama, T. Tanaka and S. Yokoyama, *Primordial black holes—perspectives in gravitational wave astronomy*, *Class. Quant. Grav.* **35** (2018) 063001 [[1801.05235](#)].
- [90] T. Nakamura, M. Sasaki, T. Tanaka and K.S. Thorne, *Gravitational waves from coalescing black hole MACHO binaries*, *Astrophys. J. Lett.* **487** (1997) L139 [[astro-ph/9708060](#)].